ELSEVIER

Physica D 92 (1996) 28–60

PHYSICA D

The reduction of complex dynamical systems using principal interaction patterns

F. Kwasniok

Max-Planck-Institut für Meteorologie, Bundesstr. 55, D-20146 Hamburg, Germany

Received 4 May 1995; revised 25 October 1995; accepted 25 October 1995
Communicated by F.H. Busse

Abstract

A method of constructing low-dimensional nonlinear models capturing the main features of complex dynamical systems with many degrees of freedom is described. The system is projected onto a linear subspace spanned by only a few characteristic spatial structures called Principal Interaction Patterns (PIPs). The expansion coefficients are assumed to be governed by a nonlinear dynamical system. The optimal low-dimensional model is determined by identifying spatial modes and interaction coefficients describing their time evolution simultaneously according to a nonlinear variational principle.

The algorithm is applied to a two-dimensional geophysical fluid system on the sphere. The models based on Principal Interaction Patterns are compared to models using Empirical Orthogonal Functions (EOFs) as basis functions. A PIP-model using 12 patterns is capable of capturing the long-term behaviour of the complete system monitored by second-order statistics, while in the case of EOFs 17 modes are necessary.

PACS: 02.60.-x; 02.70.-c; 05.45.+b; 47.11.+j; 47.27.-i; 47.32.-y; 47.52.+j; 47.54.+r
Keywords: Ordinary and partial differential equations; Galerkin methods; Low-dimensional dynamics; Pattern identification; Variational principle; Numerical optimization; Geophysical flow

1. Introduction

In various fields of research such as fluid dynamics, atmospheric sciences and other physical subjects there occur complex dynamical systems with many degrees of freedom. Frequently a model is formulated in terms of partial differential equations (PDEs) from which a system of ordinary differential equations (ODEs) is derived via a Galerkin procedure using eigenfunctions of some linear differential operator, commonly Fourier modes, as basis functions. Despite the complexity the dynamics of such systems are often confined to attractor sets of a dimension much smaller than the dimension of phase space. Coherent structures emerge; the dynamical behaviour of the system (or at least of an important part of the system representing e.g. a particular physical phenomenon one focuses on) seems to be dominated by the interaction among relatively few characteristic spatial patterns; i.e. the system is in fact in some sense low-dimensional. Hence the construction of minimal models capturing (or at least well approximating) the principal properties of the complete system is an

SSDI 0167-2789(95)00280-4

interesting task in such cases. Reduced models especially may be a helpful tool to understand the system, e.g. to gain insight in the physical driving mechanisms of particular phenomena occurring in the system.

For some PDEs (e.g. the Kuramoto–Sivashinsky equation, the Ginzburg–Landau equation and several reaction-diffusion equations under certain boundary conditions) even the existence of an inertial manifold has been established; i.e. the flow associated with these PDEs is on the attractor rigorously equivalent to that of a finite-dimensional system of ODEs. In such cases not only an approximate reduced dynamical system can be constructed but a complete finite-dimensional description of the long-term dynamics of the PDE is possible. But for most models of practical interest such proofs are not available. Moreover these theorems in general do not provide a methodology to determine the explicit numerical parametrization of such an inertial manifold. Thus, in order to actually implement a reduced model an approximation is always necessary independent of the existence of an inertial manifold.

The Fourier modes in principle allow for a complete description of the time evolution, but this description cannot be expected to be very efficient as to the number of functions involved since Fourier modes are completely general and do not take advantage of information about the particular system under consideration at all. This leads to the idea that a description in terms of characteristic patterns may be more adequate when searching for a minimal model.

How to identify such patterns is far from clear. Modes obtained from an Empirical Orthogonal Function analysis, also referred to as Principal Component analysis, Proper Orthogonal Decomposition or Karhunen–Loève expansion in the continuous case are an obvious candidate on intuitive grounds. They can be calculated quite easily as solutions of an eigenvalue problem or of a linear Fredholm integral equation in the continuous case involving second-order correlation tensors of the dynamical variables. Empirical Orthogonal Functions (EOFs) provide an optimal representation of a multivariate dynamical field in a mean least-squares sense using a given number of modes. But they a priori do not contain any information about the time evolution or the dynamical structure of the system. Of course the modes obtained from an EOF-analysis can be used and have been used to build a low-dimensional model [1–7], but they are not optimized for this purpose. In [8] the EOF approach is extended to the so called Sobolev eigenfunctions. They yield an optimal representation not only of the state itself but also of its spatial derivatives by minimizing a weighted norm containing the EOFs as a special case. But still only second-order statistics is used.

In the present paper modes which are optimal with respect to the time evolution are calculated to construct reduced models. They are obtained from a nonlinear minimization procedure based on a dynamical optimality criterion involving higher-order correlation tensors of both the state variables and their time derivatives. The method takes into account spatial as well as temporal features of the dynamical system by identifying spatial modes and interaction coefficients describing their time evolution simultaneously, in contrast to EOF-analysis which concentrates solely on spatial properties of the system and does not deal with mode interaction.

The approach pursued in this paper is similar to that described and applied to synthetic as well as experimental data in [9–12] which aims at the analysis of mode interaction in the vicinity of critical points and refers to the theory of synergetics involving unstable modes, corresponding order parameters and enslaved stable modes. In [13] the concept of Principal Interaction Patterns is applied to the description and analysis of the time evolution of baroclinic wave life cycles, a nonlinear periodic scenario in the field of atmospheric science.

The present study starts out from a chaotic two-dimensional fluid system on the rotating sphere, a crude model of the large-scale atmospheric circulation, described by a system of very many ODEs derived from a PDE (the barotropic vorticity equation) via a Fourier–Galerkin procedure. The question is addressed to what extent a system with relatively few degrees of freedom using optimized basis functions succeeds in capturing the essential dynamical behaviour of the full system. The minimal dimension of this reduced system will be found by trial and error in this case since for the barotropic vorticity equation there is no a priori knowledge

concerning the existence of an inertial manifold let alone its dimension.

The paper is organized as follows: In Section 2 the methodology is outlined in general. Then the geophysical fluid system used as an example to test and study the method is introduced. The Galerkin procedure to derive reduced systems from this equation is described. In Section 5 the method of constructing an optimal low-dimensional system is given in detail. Then the results are presented in Section 6. Some emphasis is put on the comparison with reduced models based on EOFs. The paper is concluded in Section 7. In the Appendix some numerical details of the algorithm are discussed.

2. Methodology

The algorithm follows a general concept proposed by Hasselmann [14] which is slightly modified in this study. Consider a nonlinear autonomous dynamical system of first order in N-dimensional phase space:

$$\dot{\Phi} = F(\Phi)\,, \quad \Phi = (\Phi_1, \cdots, \Phi_N) \tag{1}$$

N may be quite large (10^2–10^5); e.g. think of a system of differential equations originating from a partial differential equation via a Galerkin procedure (cf. Section 4.1). The high-dimensional dynamical field $\Phi(t)$ is projected onto a limited number of time-independent spatial modes which will be called Principal Interaction Patterns (PIPs):

$$\Phi(t) = \sum_{i=1}^{L} z_i(t)\, p_i + \rho\,, \quad L \ll N \tag{2}$$

ρ denotes the vector of the residual error. In matrix notation Eq. (2) reads

$$\Phi = Pz + \rho \tag{3}$$

where P is the $(N \times L)$-matrix with the PIPs as its columns. The time dependence is suppressed in the notation from now on. For a given set of patterns the vector of expansion coefficients z at each time is defined by requiring that the squared error in the representation of the state vector

$$\rho^t M \rho = (\Phi - Pz)^t M (\Phi - Pz) \tag{4}$$

measured in some metric M be minimized. This constitutes a linear least-squares problem which can be solved uniquely using the Moore–Penrose generalized inverse of P with respect to M

$$z = P^+ \Phi = (P^t M P)^{-1} P^t M \Phi \tag{5}$$

or in other terms

$$z = P^{*t} M \Phi \tag{6}$$

with P^* being the $(N \times L)$-matrix of adjoint patterns

$$P^* = P(P^t M P)^{-1} \tag{7}$$

defined as the set of vectors p_i^* which lie in the linear subspace spanned by the PIPs and which are orthonormal to them with respect to the metric M:

$$p_i^{*t} M p_j = \delta_{ij} \tag{8}$$

The dynamics of the time-dependent coefficients z are assumed to be governed by an autonomous system of L first-order differential equations

$$\dot{z}^{\mathrm{pip}} = G(z;\sigma) \tag{9}$$

depending on a set of adjustable parameters $\sigma = (\sigma_1, \cdots, \sigma_R)$. The dynamical system is specified as a member of a model class suitably chosen based on some physical knowledge or reasoning about the character of the system to model. $\dot{z}^{\mathrm{pip}}$ denotes the vector of the tendencies of the PIP-amplitudes as given by the low-dimensional PIP-model in contradistinction from the tendencies given by the full system $\dot{z} = P^+\dot{\Phi} = P^+ F(\Phi)$. The optimal set of patterns and the optimal parameters are determined simultaneously by minimizing the error in the derivative of the PIP-coefficients between the reduced system and the entire system in a mean least-squares sense:

$$\begin{aligned} Q(P,\sigma) &= \overline{\left(\dot{z}^{\mathrm{pip}} - \dot{z}\right)^t \widetilde{M} \left(\dot{z}^{\mathrm{pip}} - \dot{z}\right)} \\ &= \overline{\left[G(z(P),\sigma) - P^+\dot{\Phi}\right]^t \widetilde{M} \left[G(z(P),\sigma) - P^+\dot{\Phi}\right]} = \mathrm{Min.} \end{aligned} \tag{10}$$

The overbar denotes ensemble averaging which is equivalent to time averaging if ergodicity is assumed. In practice it will be replaced by a sum over a discrete and finite time series obtained from a long-term integration of the full system of Eq. (1). The metric $\widetilde{M}$ may be chosen as the inverse of the covariance matrix of the derivatives of the PIP-amplitudes to guarantee equal weighting of all modes:

$$\widetilde{M} = \left(P^+ \Pi P^{+t}\right)^{-1} = P^t M P (P^t M \Pi M P)^{-1} P^t M P \tag{11}$$

Π is the covariance matrix of the derivatives of the full system:

$$\Pi_{\alpha\beta} = \overline{\dot{\Phi}_\alpha \dot{\Phi}_\beta}, \quad \alpha,\beta = 1,\cdots,N \tag{12}$$

In principle the parameters σ are independent variables in the minimization problem. However, in this study as a first step they will be (mainly) connected to the patterns by a Galerkin procedure (cf. Section 4.2). Eq. (10) in general poses a high-dimensional nonlinear minimization problem which has to be solved numerically by iterative techniques.

In the case of a linear function G the Principal Interaction Patterns reduce to the Principal Oscillation Patterns (POPs) (cf. [14]). The POP-analysis may be a helpful tool if there is evidence (from other techniques or from a priori knowledge) that the system under consideration or a considerable part of the system can be adequately modelled by linear dynamics (perhaps when restricting oneself to certain time scales, e.g. think of atmospheric or oceanic processes on time scales from months up to decades). The method then extracts principal modes of oscillation of the system and corresponding frequencies and decay constants or growth rates, respectively. In a simplified version of POP-analysis the linear subspace spanned by the modes of oscillation is not determined in an optimal way simultaneously with the model parameters according to the variational principle of Eq. (10) but is fixed as the subspace of some leading EOFs. Then an optimal linear model in this known subspace is fitted to the time series; i.e. a system reduction is achieved just by the neglect of higher EOFs prior to the POP-analysis and is not incorporated in the algorithm in a dynamically motivated manner. This latter kind of POP-analysis is a widely used tool in the fields of meteorology and climate research for the analysis and interpretation of multivariate data sets (either from observations or from numerical simulations with high-resolution models) commonly focussing on particular physical phenomena occurring on particular time scales. See [15] and many references therein for an extensive account on Principal Oscillation Patterns and various applications.

The present paper illustrates the nonlinear case of the concept of Principal Interaction Patterns.

3. The two-dimensional fluid system

In this study a vertically homogeneous layer of incompressible fluid over topography on the rotating sphere is considered. If the approximations of shallowness and quasigeostrophy are applied the flow can be described by a streamfunction $\Psi(\lambda, \mu)$ which obeys the non-divergent barotropic quasigeostrophic potential vorticity equation:

$$\frac{\partial}{\partial t}\left(\Delta\Psi - \frac{1}{\lambda_R^2}\Psi\right) + \mathcal{J}(\Psi, \Delta\Psi + f + h) = -\kappa_1\Delta\Psi - \kappa_2\Delta^4\Psi + \Delta\widetilde{\Psi} \tag{13}$$

λ and $\mu = \sin\vartheta$ denote the longitudinal and latitudinal coordinates on the sphere, respectively. Δ and $\mathcal{J}$ stand for the Laplacian and the Jacobian operator, respectively:

$$\Delta = \frac{1}{1-\mu^2}\frac{\partial^2}{\partial\lambda^2} + \frac{\partial}{\partial\mu}\left[(1-\mu^2)\frac{\partial}{\partial\mu}\right], \tag{14}$$

$$\mathcal{J}(a, b) = \frac{\partial a}{\partial\lambda}\frac{\partial b}{\partial\mu} - \frac{\partial a}{\partial\mu}\frac{\partial b}{\partial\lambda} \tag{15}$$

$f = 2\mu$ is the Coriolis parameter. h represents an effective topography which is related to the real dimensional topography of the earth h_{dim} by $h = 2\sin(\vartheta_0)A_0\frac{h_{\text{dim}}}{H}$; ϑ_0 being some average latitude taken to be 45°N; H being a scale height of the atmosphere (H = 10 km) and A_0 being a scaling factor set to 0.2. The linear damping represents surface friction; the coefficient κ_1 has a value corresponding to a damping time scale of 15 days. The scale selective horizontal diffusion term parametrizes the effect of eddies on very small non-resolved spatial scales onto the resolved scales (cf. Section 4.1). $\widetilde{\Psi}$ is a constant forcing streamfunction which can be interpreted as thermal forcing owing to solar radiation. The Rossby radius of deformation λ_R is set to infinity in this study (rigid lid approximation).

The zonal and meridional velocity of the flow, respectively, is given by $u = -\sqrt{1-\mu^2}\frac{\partial\Psi}{\partial\mu}$ and $v = \frac{1}{\sqrt{1-\mu^2}}\frac{\partial\Psi}{\partial\lambda}$. $\zeta = \Delta\Psi$ is the relative vorticity. Eq. (13) has been nondimensionalized using the radius of the earth as unit of length and the inverse of the angular velocity of the earth as unit of time. The barotropic vorticity equation may be regarded as the crudest model of large-scale atmospheric dynamics. For a rigorous derivation of Eq. (13) from the three-dimensional Navier–Stokes equations see e.g. [16–18].

It can be shown that Eq. (13) in the absence of friction and forcing conserves kinetic energy

$$\text{KE} = \tfrac{1}{2}\left(\langle u, u\rangle + \langle v, v\rangle\right) = -\tfrac{1}{2}\langle\Psi, \Delta\Psi\rangle \tag{16}$$

and in the absence of friction, forcing and topography conserves enstrophy

$$\text{ENS} = \tfrac{1}{2}\langle\zeta, \zeta\rangle = \tfrac{1}{2}\langle\Delta\Psi, \Delta\Psi\rangle \tag{17}$$

where $\langle\cdot,\cdot\rangle$ signifies the scalar product

$$\langle a, b\rangle = \frac{1}{4\pi}\int a(\lambda, \mu)b(\lambda, \mu)\, d\Omega = \frac{1}{4\pi}\int_{-1}^{1}\int_{0}^{2\pi} a(\lambda, \mu)b(\lambda, \mu)\, d\lambda d\mu \tag{18}$$

4. Derivation of truncated models

4.1. Spectral basis

The streamfunction, the topography and the forcing are expanded into a triangularly truncated series of spherical harmonics. The vorticity equation is considered on the northern hemisphere. Only modes with odd parity are used in the expansion. This corresponds to the boundary condition $v = 0$ at the equator (no flow across the equator). For the streamfunction the expansion reads:

$$\Psi(\lambda, \mu, t) = \sum_{\alpha=1}^{N} \Psi_\alpha(t)\, Y_\alpha(\lambda, \mu) \tag{19}$$

The functions Y_α are the real spherical harmonics up to total wavenumber $n_{\max}$:

$$\{Y_\alpha; \alpha = 1, \cdots, N\} = \left\{P_n^0; n = 1, \cdots, n_{\max}; n \text{ odd}\right\} \cup \left\{\sqrt{2}\, P_n^m \cos(m\lambda), \sqrt{2}\, P_n^m \sin(m\lambda); n = 1, \cdots, n_{\max}; m = 1, \cdots, n; n + m \text{ odd}\right\}$$

P_n^m denote associated Legendre functions of the first kind defined by

$$P_n^m(\mu) = \sqrt{(2n+1)\frac{(n-m)!}{(n+m)!}}\frac{(1-\mu^2)^{\frac{m}{2}}}{2^n n!}\left(\frac{d}{d\mu}\right)^{n+m}(\mu^2-1)^n, \quad m \geq 0 \tag{20}$$

normalized in a way that

$$\langle Y_\alpha, Y_\beta \rangle = \delta_{\alpha\beta} \tag{21}$$

holds. Ψ_α are the corresponding expansion coefficients. The number of modes in the expansion is $N = \frac{1}{2} n_{\max}(n_{\max} + 1)$. The spherical harmonics are eigenfunctions of the Laplacian operator:

$$\Delta Y_\alpha = -n(n+1) Y_\alpha \tag{22}$$

Insertion of the expansion of Eq. (19) into Eq. (13) yields a system of N ODEs. The system of equations is integrated in time using the transform method proposed by Orszag [19] and a standard ODE integrator of high order. With the transform method the spectral components of a Jacobian term

$$\left\langle Y_\alpha, \mathcal{J}\left(\sum_{\beta=1}^{N} a_\beta Y_\beta, \sum_{\gamma=1}^{N} b_\gamma Y_\gamma\right)\right\rangle, \quad \alpha = 1, \cdots, N$$

are calculated involving only $\mathcal{O}(n_{\max}^3)$ operations (or $\mathcal{O}(N^{3/2})$ operations, respectively). The relevant spatial derivatives are evaluated on a grid in physical space using a Fourier transform in the longitudinal direction and a Legendre transform in the latitudinal direction. The nonlinear terms are formed directly on the grid. Then the inverse transforms are used to return to spectral space. The grid consists of K_1 equally spaced mesh points in the longitudinal direction (corresponding to the trapezoidal quadrature rule) and K_2 mesh points in the latitudinal direction (excluding the poles) located at the zeros of the Legendre polynomial $P_{K_2}^0$ (corresponding to the Gauss–Legendre quadrature rule). Considering the maximum wavenumber of the Fourier series and the maximum degree of the Legendre polynomials occurring in the algorithm and using the exactness properties of the trapezoidal and the Gaussian quadrature rule, respectively, it may be shown that K_1 has to be at least

$3n_{\max}+1$ and K_2 has to be at least the smallest integer greater or equal $\frac{1}{2}(3n_{\max}+1)$ in order to obtain an exact representation of the nonlinear terms. See [19,20] for the detailed formulae of the transform method.

In this study the expansion is truncated at wavenumber $n_{\max}=21$. This yields a linear subspace $\mathcal{H}$ spanned by $N=231$ real modes. The coefficient κ_2 of the scale selective diffusion term is set to a value representing a damping time scale of 3 days in the smallest scale (wavenumber 21). The diffusion term accounts for the neglected interactions with the unresolved modes. Their mean influence on the resolved modes can be parametrized by a linear damping. The external forcing $\widetilde{\Psi}$ is specified from a 500 hPa streamfunction analysis data set in a way that the system has a realistic mean state and a variance pattern similar to that of 10 days running mean streamfunction fields. See [7] for the detailed procedure.

Test calculations using various truncation limits $n_{\max}$ and referring to the turbulent kinetic energy spectrum as a simple benchmark revealed that the dynamical behaviour of the truncated system converges sufficiently at about $n_{\max}=20$. The results on the convergence properties of the spectral expansion are given in Fig. 8 and discussed in Section 6.1 together with the results for the reduced models based on PIPs. The specific truncation limit of wavenumber 21 is motivated by reasons of computational efficiency. The longitudinal dimension of the transform grid K_1 is then 64 which is a power of 2 and therefore allows for the use of a particularly efficient Fast Fourier Transform algorithm in the transform method. In the latitudinal direction the grid has $K_2=32$ mesh points (16 on the northern hemisphere).

The finite subspace $\mathcal{H}$ spanned by the 231 Fourier modes is of course not an inertial manifold of Eq. (13) in a rigorous mathematical sense but it turns out to be sufficient to capture the long-term behaviour of the solution as far as first and second moments are concerned. The system exhibits chaotic behaviour detected by continuous power spectra and positive Lyapunov exponents (calculated with the method proposed by Shimada and Nagashima [21]). It reproduces some essential features of atmospheric behaviour quite well (red power spectrum, energy and enstrophy spectra, preferred flow patterns). Therefore the system of 231 ordinary differential equations can be regarded as a rough model of the large-scale atmospheric circulation. It will be the complex system we start out from to derive reduced models.

It is convenient to separate the flow Ψ into the time-independent mean flow $\overline{\Psi}$ and the anomalies Ψ':

$$\Psi(\lambda,\mu,t)=\overline{\Psi}(\lambda,\mu)+\Psi'(\lambda,\mu,t)=\sum_{\alpha=1}^{N}\left[\overline{\Psi}_\alpha+\Psi'_\alpha(t)\right]Y_\alpha(\lambda,\mu) \tag{23}$$

From now on all quantities and operators are replaced by their projection onto $\mathcal{H}$. Hence $\Psi,\overline{\Psi},\Psi',\dot{\Psi},\widetilde{\Psi},f$ and h have to be read as vectors of spherical harmonics coefficients in N-dimensional space; Δ as a diagonal $(N\times N)$-matrix with the eigenvalues of Eq. (22) on its diagonal and $\mathcal{J}$ as a nonlinear map from $\mathcal{H}\times\mathcal{H}$ into $\mathcal{H}$. The scalar product $\langle\cdot,\cdot\rangle$ corresponds to the canonical scalar product in $\mathcal{R}^N$ because of Eq. (21).

For completeness it should be stated that the dynamic equations for the Ψ'_α form a system of the type

$$\dot{\Psi}'_\alpha=\tfrac{1}{2}\sum_{\beta,\gamma=1}^{N}A^{\mathrm{sh}}_{\alpha\beta\gamma}\Psi'_\beta\Psi'_\gamma+\sum_{\beta=1}^{N}B^{\mathrm{sh}}_{\alpha\beta}\Psi'_\beta+C^{\mathrm{sh}}_\alpha \tag{24}$$

with negative definite matrix B^{sh}; a forced, dissipative system with quadratic nonlinearity. The quadratic term represents nonlinear wave-wave interactions; the linear term includes mean-wave interactions, the Coriolis effect, the topography and the friction terms; the forcing term is formed by the external forcing and the time-independent terms arising from the separation into mean flow and deviations from it. The superscript sh signifies that the quantities refer to spherical harmonics. Note that the tensors of coefficients $A^{\mathrm{sh}},B^{\mathrm{sh}}$ and C^{sh} are not used explicitly in the integration of the truncated system. They could be obtained from a straightforward

spectral expansion of Eq. (13) involving the coupling integral $I_{\alpha\beta\gamma} = \langle Y_\alpha, \mathcal{J}(Y_\beta, Y_\gamma)\rangle$; but a calculation of the nonlinear terms by direct summation would require $\mathcal{O}(N^{5/2})$ operations for each evaluation of the right hand side of Eq. (24) (taking into account the selection rules for the coupling integral) compared to $\mathcal{O}(N^{3/2})$ operations when using the transform method.

4.2. Principal interaction patterns

Now we consider an L-dimensional subspace $\mathcal{P}$ in $\mathcal{H}$ spanned by the Principal Interaction Patterns. The streamfunction anomalies are expanded into a series of PIPs:

$$\Psi = \overline{\Psi} + \sum_{i=1}^{L} z_i p_i \tag{25}$$

The vector of expansion coefficients is

$$z = P^+ \Psi' \tag{26}$$

A reduced model is then defined by a projection of the terms in Eq. (13) onto PIP-space:

$$P^+\dot{\Psi} + P^+\Delta^{-1}\mathcal{J}\left[\overline{\Psi} + PP^+\Psi', \Delta\left(\overline{\Psi} + PP^+\Psi'\right) + f + h\right] = -\kappa_1 P^+\left(\overline{\Psi} + \Psi'\right) - \kappa_2 P^+\Delta^3\left(\overline{\Psi} + PP^+\Psi'\right) + P^+\widetilde{\Psi} \tag{27}$$

This yields a system of ordinary differential equations for the PIP-amplitudes z with the same structure as the complete system represented by Eq. (24):

$$\dot{z}_i^{\mathrm{pip}} = G_i = \tfrac{1}{2}\sum_{j,k=1}^{L} A_{ijk} z_j z_k + \sum_{j=1}^{L} B_{ij} z_j + C_i \tag{28}$$

The coefficients are given by

$$A_{ijk} = -\langle p_i^*, M\Delta^{-1}\left[\mathcal{J}(p_j, \Delta p_k) + \mathcal{J}(p_k, \Delta p_j)\right]\rangle, \tag{29}$$

$$B_{ij} = -\langle p_i^*, M\left(\Delta^{-1}\left[\mathcal{J}(\overline{\Psi}, \Delta p_j) + \mathcal{J}(p_j, \Delta\overline{\Psi} + f + h)\right] + \kappa_1 p_j + \kappa_2 \Delta^3 p_j\right)\rangle, \tag{30}$$

$$C_i = \langle p_i^*, M\left(\widetilde{\Psi} - \Delta^{-1}\mathcal{J}(\overline{\Psi}, \Delta\overline{\Psi} + f + h) - \kappa_1\overline{\Psi} - \kappa_2\Delta^3\overline{\Psi}\right)\rangle \tag{31}$$

$\dot{z}^{\mathrm{pip}}$ denotes the tendencies of the PIP-amplitudes as given by the truncated model in contradistinction from the exact tendencies $\dot{z} = P^+\dot{\Psi}$. For completeness it is stated here that this kind of truncation is equivalent to a projection of the tensors of interaction coefficients of the full system:

$$A_{ijk} = \sum_{\alpha,\beta,\gamma=1}^{N} P_{i\alpha}^+ P_{\beta j} P_{\gamma k} A_{\alpha\beta\gamma}^{\mathrm{sh}}, \tag{32}$$

$$B_{ij} = \sum_{\alpha,\beta=1}^{N} P_{i\alpha}^+ P_{\beta j} B_{\alpha\beta}^{\mathrm{sh}}, \tag{33}$$

$$C_i = \sum_{\alpha=1}^{N} P_{i\alpha}^+ C_\alpha^{\mathrm{sh}} \tag{34}$$

The formulae (32)–(34) are not used in the actual calculations. For the evaluation of the interaction coefficients of the reduced model see Appendix B.

The elements of the tensors A, B and C form the set of parameters σ introduced in Section 2. Hence the parameters in this case are connected to the patterns rather than determined independently from them.

In the present calculations three different metrics M for defining the projection are considered which have particular physical meaning: $M_1 = 1$, the squared anomaly streamfunction metric; $M_2 = -\Delta$, the turbulent kinetic energy metric; and $M_3 = \Delta^2$, the turbulent enstrophy and squared anomaly vorticity metric.

Note that Eqs. (25)–(34) are completely general; they hold for any L-dimensional subspace $\mathcal{P} \subseteq \mathcal{H}$ spanned by L arbitrary linearly independent modes. Especially, if the patterns are chosen as spherical harmonics and M_1 is chosen as metric one returns to the corresponding coupling coefficients of the full system in Eq. (24).

A special choice of PIPs are the EOFs. In the following subsection the definition and the main properties of EOFs are reviewed briefly.

4.3. Empirical orthogonal functions

Starting out from an N-dimensional state vector $\Phi(t)$ one may ask for an expansion using only S spatial modes ($S < N$) which converges optimally fast in the sense that the mean squared error in the representation of Φ

$$\mathrm{mse}_S = \overline{\left(\Phi - \sum_{\alpha=1}^{S} \widehat{\Phi}_\alpha e_\alpha\right)^t \overline{M} \left(\Phi - \sum_{\alpha=1}^{S} \widehat{\Phi}_\alpha e_\alpha\right)} \tag{35}$$

with

$$\widehat{\Phi}_\alpha = e_\alpha^t \overline{M} \Phi \tag{36}$$

be minimized subject to

$$e_\alpha^t \overline{M} e_\beta = \delta_{\alpha\beta}, \quad \alpha, \beta = 1, \cdots, S \tag{37}$$

$\overline{M}$ may be an arbitrary symmetric, positive definite metric. It is well known that the solution to this minimization problem is given by the eigenvectors corresponding to the S largest eigenvalues of the eigenvalue problem

$$\Gamma \overline{M} e_\alpha = \lambda_\alpha^{\mathrm{eof}} e_\alpha \tag{38}$$

Γ being the matrix of second moments of Φ:

$$\Gamma_{\alpha\beta} = \overline{\Phi_\alpha \Phi_\beta}, \quad \alpha, \beta = 1, \cdots, N \tag{39}$$

The matrix $\Gamma \overline{M}$ as a product of symmetric, positive definite matrices can be diagonalized in a real basis and has only real and positive eigenvalues. The amplitudes of the EOFs $\widehat{\Phi}_\alpha$ are pairwise uncorrelated and the second moment of each is given by the corresponding eigenvalue:

$$\overline{\widehat{\Phi}_\alpha \widehat{\Phi}_\beta} = \delta_{\alpha\beta} \lambda_\alpha^{\mathrm{eof}} \tag{40}$$

The mean squared error is then given by

$$\mathrm{mse}_S = \sum_{\alpha=S+1}^{N} \lambda_\alpha^{\mathrm{eof}} \tag{41}$$

EOFs may be calculated either from the full state vector Φ or only from the anomalies $\Phi' = \Phi - \overline{\Phi}$. See [22] for an extensive overview on the mathematical properties of EOF-analysis.

Note that the EOFs are only optimal for capturing as much variance as possible with a given number of modes. To construct a reduced system it is necessary to describe the time evolution of the modes chosen as basis functions. For this purpose one has to model not only the state itself, but also the terms occurring in the dynamical equation governing the time evolution, e.g. the spatial derivatives (cf. [8]). This is not implied with EOFs. The optimality criterion expressed in Eqs. (35)–(37) does not refer to dynamics at all. Nevertheless the EOFs may be regarded as an attractive candidate for a set of basis functions in a reduced model since they already take into account the characteristics of the system under consideration to a large extent (the structure of the second moments) compared to eigenfunctions of a linear differential operator, here spherical harmonics, which are completely general.

4.4. *Conserved quantities of truncated models*

In view of the conserved integral quantities of Eq. (13) one may ask if this conservation properties are adopted by truncated systems. Since in the present study the mean state is prescribed and only the streamfunction anomalies are expanded into a series of PIPs (cf. Eq. (25)) statements can only be formulated for the turbulent kinetic energy and the turbulent enstrophy instead of the total kinetic energy and enstrophy. The turbulent kinetic energy of the spectral model represented by Eq. (24) is

$$\mathrm{TKE} = -\tfrac{1}{2}\langle \Psi', \Delta\Psi' \rangle \tag{42}$$

the turbulent enstrophy is

$$\mathrm{TENS} = \tfrac{1}{2}\langle \Delta\Psi', \Delta\Psi' \rangle \tag{43}$$

The corresponding projected quantities in L-dimensional PIP-space are

$$\mathrm{TKE}^{\mathrm{pip}} = -\tfrac{1}{2}\langle PP^{+}\Psi', \Delta PP^{+}\Psi' \rangle = -\tfrac{1}{2} z^{t} P^{t} \Delta P z \tag{44}$$

and

$$\mathrm{TENS}^{\mathrm{pip}} = \tfrac{1}{2}\langle \Delta PP^{+}\Psi', \Delta PP^{+}\Psi' \rangle = \tfrac{1}{2} z^{t} P^{t} \Delta^{2} P z \tag{45}$$

For reduced systems based on spherical harmonics the nonlinear wave-wave interactions, the Coriolis term and the topography term in Eq. (28) conserve both the projected turbulent kinetic energy and (except for the topography) the projected turbulent enstrophy for all three metrics considered (especially the full system of Eq. (24) does). As a consequence the flow in phase space associated with the nonlinear terms is divergence-free (Liouvillian property). This does not hold in the case of general patterns. This difference is due to the fact that in case of spherical harmonics the projection operator PP^{+} and Δ commute because of Eq. (22), whereas in the general case they do not. Then the conservation properties depend on the metric M used in the projection procedure. If the kinetic energy metric M_2 is used the quadratic terms, the Coriolis and the topography terms of the PIP-model conserve the truncated turbulent kinetic energy $\mathrm{TKE}^{\mathrm{pip}}$, if the enstrophy metric M_3 is used the truncated turbulent enstrophy $\mathrm{TENS}^{\mathrm{pip}}$ is conserved by the nonlinear interactions and the Coriolis term; in the case of the norm streamfunction metric M_1 no conserved quantity exists. It is in general not possible to conserve both turbulent kinetic energy and turbulent enstrophy by the quadratic terms in a reduced model defined according to the formulae (27)–(31). Also the divergence of the nonlinear terms generally does not vanish. Actually there are alternative formulations of truncated models which allow for conservation of both

integral quantities (see [7]) but these are unfavourable for other reasons and are not considered here. If the full streamfunction is expanded into a series of PIPs analogous statements to those mentioned above hold for the truncated total kinetic energy and enstrophy instead of $\mathrm{TKE}^{\mathrm{pip}}$ and $\mathrm{TENS}^{\mathrm{pip}}$. Note that the existence of at least one conserved quantity for the quadratic interactions guarantees that the solutions of the reduced system are bounded for all times. The conservation statements can be proven quite easily with the help of Eq. (5) and the following identities valid for all $a, b \in \mathcal{H}$:

$$\langle a, \mathcal{J}(a,b)\rangle = \langle b, \mathcal{J}(a,b)\rangle = 0 \tag{46}$$

$$\langle a, \Delta b\rangle = \langle \Delta a, b\rangle \tag{47}$$

$$\langle a, \mathcal{J}(b,f)\rangle = -\langle \mathcal{J}(a,f), b\rangle \tag{48}$$

5. Determination of the optimal truncated system

We now seek a reduced system which is optimal in the sense of the variational principle expressed in Eq. (10). Since for a given set of patterns the parameters are determined by the projection procedure the components of the patterns are the only independent variables and the problem is actually to identify an optimal L-dimensional linear subspace $\mathcal{P}$ in $\mathcal{H}$.

5.1. Uniqueness of the PIP-model

It is evident that the Principal Interaction Patterns are only determined to within a linear transformation. Consider an arbitrary regular linear transformation T in L-dimensional space and a matrix of patterns P. The transformed set of patterns is then $P' = PT$, the corresponding vector of expansion coefficients is $z' = T^{-1}z$. The interaction coefficients A, B and C are transformed according to the rules for tensors of third, second and first order, respectively:

$$A'_{ijk} = \sum_{l,m,n} T^{-1}_{il} T_{mj} T_{nk} A_{lmn}\,, \tag{49}$$

$$B'_{ij} = \sum_{m,n} T^{-1}_{im} T_{nj} B_{mn}\,, \tag{50}$$

$$C'_{i} = \sum_{m} T^{-1}_{im} C_{m} \tag{51}$$

The error function Q is invariant under this transformation: $Q(P') = Q(P)$.

To eliminate this gauge freedom one has to refer to some normal form for the matrix of patterns. One possibility to do so is to impose the constraints that the patterns be orthonormal with respect to M, that their amplitudes be uncorrelated with the patterns ordered by descending mean squared amplitude and that the coefficients C_i be always positive:

$$p_i^{\dagger} M p_j = \delta_{ij}\,, \tag{52}$$

$$\overline{z_i z_j} = p_i^{*t} M \Gamma M p_j^* = \lambda_i^{\mathrm{pip}} \delta_{ij}, \quad \lambda_i^{\mathrm{pip}} > \lambda_{i+1}^{\mathrm{pip}} \tag{53}$$

$$C_i \geq 0 \tag{54}$$

Besides this gauge freedom the existence of several sets of patterns sharing the same value of the error function cannot be excluded rigorously since Q is highly nonlinear in P but generically does not occur.

Note that the constraints of Eqs. (52) and (53) are imposed here only to guarantee a numerically stable and efficient minimization procedure. There are no further implications of them. Especially a dynamical interpretation of the patterns is in general neither facilitated nor limited by these constraints. After the minimization the obtained patterns and corresponding interaction tensors may be linearly transformed in a different way always keeping the same dynamical information. E.g. in the linear case (POPs) it is adequate to apply a complex transformation which diagonalizes the matrix B and provides complex conjugate pairs of patterns since this is a kind of natural coordinate system for linear systems; the results of a POP- analysis then can be interpreted dynamically in an illustrative way in terms of frequencies and decay constants and oscillation patterns with amplitudes and phases. The patterns are then in general neither orthogonal nor uncorrelated. But in the case of a nonlinear system there is in general no obvious linear transformation which allows for a lucid dynamical interpretation of the obtained reduced system. Therefore the PIPs in this study will always be orthonormal and uncorrelated just to refer to some standardized normal form.

5.2. *Reduction of dimension using EOFs*

The projection procedure is carried out in two steps. In order to reduce the number of variables in the minimization procedure the Principal Interaction Patterns and therewith also the adjoint patterns are assumed to lie in the S-dimensional subspace $\mathcal{E}$ spanned by the first S EOFs calculated from the streamfunction anomalies with respect to M ($\overline{M} = M; L \leq S \leq N; \mathcal{P} \subseteq \mathcal{E} \subseteq \mathcal{H}$):

$$p_i = \sum_{\alpha=1}^{S} \widehat{P}_{\alpha i} e_\alpha \quad \text{or} \quad P = E\widehat{P} \tag{55}$$

E is the $(N \times S)$-matrix of the first S EOFs; $\widehat{P}$ is the $(S \times L)$-matrix with the PIPs $\widehat{p}$ expressed in terms of their EOF-coefficients as its column vectors. The EOFs are orthonormal with respect to M ($e_\alpha^t M e_\beta = \delta_{\alpha\beta}$). It is sufficient then to consider the projection of the system onto these S EOFs. Let $\widehat{\Psi}$ and $\widehat{\dot{\Psi}}$ be the vectors of EOF-coefficients of the streamfunction anomalies and their time derivatives, respectively:

$$\widehat{\Psi} = E^t M \Psi', \tag{56}$$

$$\widehat{\dot{\Psi}} = E^t M \dot{\Psi}' \tag{57}$$

The vector of PIP-coefficients is then

$$z = \widehat{P}^+ \widehat{\Psi} \tag{58}$$

with

$$\widehat{P}^+ = \widehat{P}^{*t} = (\widehat{P}^t \widehat{P})^{-1} \widehat{P}^t \tag{59}$$

$\widehat{P}^*$ being the $(S \times L)$-matrix of adjoint patterns in the EOF-representation.

This restriction in the choice of the patterns is motivated as follows: First, it is simply a necessity to reduce the number of variables in the minimization procedure by restricting the choice of patterns somehow to stay within the limits of available computer power. Moreover the study of Selten [7] referring to the same fluid system and finding a reduced model based on 20 EOFs capable of both capturing the global behaviour of the system and predicting the flow for some time supports the expectation that the EOFs actually are already a good approximation to the optimal dynamical modes and that the PIPs will have largest contributions from leading EOFs.

5.3. The variational principle

The variational principle now reads:

$$Q(\widehat{P}) = \overline{\left(\dot{z}^{\mathrm{pip}} - \dot{z}\right)^t \widetilde{M} \left(\dot{z}^{\mathrm{pip}} - \dot{z}\right)}$$
$$= \overline{\left[G\left(z(\widehat{P}), \sigma(\widehat{P})\right) - \widehat{P}^{+}\widehat{\dot{\Psi}}\right]^t \widetilde{M}(\widehat{P}) \left[G\left(z(\widehat{P}), \sigma(\widehat{P})\right) - \widehat{P}^{+}\widehat{\dot{\Psi}}\right]} = \mathrm{Min.} \tag{60}$$

subject to

$$\widehat{p}_i^t \widehat{p}_j = \delta_{ij}\,, \tag{61}$$

$$\overline{z_i z_j} = \widehat{p}_i^{*t} \widehat{\Gamma} \widehat{p}_j^{*} = \delta_{ij} \lambda_i^{\mathrm{pip}}\,, \quad \lambda_i^{\mathrm{pip}} > \lambda_{i+1}^{\mathrm{pip}}\,, \tag{62}$$

$$C_i \geq 0 \tag{63}$$

with

$$\widetilde{M} = \widehat{P}^t \widehat{P} (\widehat{P}^t \widehat{\Pi} \widehat{P})^{-1} \widehat{P}^t \widehat{P}\,, \tag{64}$$

$$\widehat{\Gamma} = E^t M \Gamma M E\,, \tag{65}$$

$$\widehat{\Pi} = E^t M \Pi M E \tag{66}$$

For the patterns spanning the S-dimensional subspace $\mathcal{E}$ one has the same gauge freedom as with the PIPs. For numerical reasons it is convenient actually not to work with the EOFs themselves but with a set of patterns E° which is related to the EOFs by an orthonormal linear transformation U in S-dimensional space ($E = E^\circ U$) chosen in a way that $\widehat{\Pi}^\circ = E^{\circ t} M \Pi M E^\circ = U \widehat{\Pi} U^t$ becomes diagonal while still preserving the orthonormality of the patterns ($e_\alpha^{\circ t} M e_\beta^\circ = \delta_{\alpha\beta}$). The corresponding matrix of PIPs is then $\widehat{P}^\circ = U\widehat{P}$; the matrix of adjoint patterns is $\widehat{P}^{\circ +} = \widehat{P}^{+} U^t$. $\widehat{\Psi}$, $\widehat{\dot{\Psi}}$ and $\widehat{\Gamma}$ are transformed according to $\widehat{\Psi}^\circ = U\widehat{\Psi}$, $\widehat{\dot{\Psi}}^\circ = U\widehat{\dot{\Psi}}$ and $\widehat{\Gamma}^\circ = U\widehat{\Gamma}U^t$, respectively.

See the Appendix for details on the calculation techniques of the minimization procedure.

5.4. Ill-conditioning and stability of the pattern identification

When dealing with chaotic systems one may ask about the stability of the pattern identification from a finite time series. There are two potential sources of errors in the algorithm: First, the EOFs of the system are not exactly known but only estimated from a finite sample of data, secondly, the nonlinear minimization to determine the PIPs also refers only to a finite sample of data. The latter one causes difficulties especially in the case that the minimization problem is ill-posed, as one expects for chaotic systems.

In the following the sampling problem in the estimation of EOFs is sketched briefly. The discussion is restricted to the case $\overline{M} = 1$ (symmetric eigenvalue problem). The general case of Eq. (38) is related to a symmetric eigenvalue problem by a similarity transformation with the matrix $\overline{M}^{1/2}$ and can be treated in an analogous manner. Let Γ be the exact covariance matrix of the system, $\widetilde{\Gamma}$ a symmetric matrix of perturbations due to the sampling error and ε a small parameter. Then the perturbed eigenvalue problem is:

$$\left(\Gamma + \varepsilon\widetilde{\Gamma}\right)\left(e_\alpha + \widetilde{e}_\alpha\right) = \left(\lambda_\alpha^{\mathrm{eof}} + \widetilde{\lambda}_\alpha^{\mathrm{eof}}\right)\left(e_\alpha + \widetilde{e}_\alpha\right) \tag{67}$$

Classical perturbation theory for symmetric linear operators in the generic non-degenerated case yields for the errors in the eigenfunctions to first order:

$$\widetilde{e}_\alpha = \varepsilon \sum_{\beta \neq \alpha} \frac{e_\alpha^t \widetilde{\Gamma} e_\beta}{\lambda_\alpha^{\mathrm{eof}} - \lambda_\beta^{\mathrm{eof}}} e_\beta + \mathcal{O}(\varepsilon^2) \tag{68}$$

Hence mixing occurs mainly among neighbouring EOFs. The estimation of the subspace of the first S EOFs is thus much more stable than the estimation of individual higher modes. Suppose a relevant subspace of S EOFs contributing to the PIPs within a certain accuracy. Then this subspace can be assumed to be covered independent of the data sample by working with S' EOFs, S' slightly larger than S. For a more detailed discussion of the sampling problem see North et al. [23].

The minimization problem turns out to be ill-posed. The Hessian matrix of the error function, or precisely the approximate Hessian matrix generated by the Quasi-Newton algorithm used to perform the numerical minimization, is ill-conditioned in the vicinity of the solution. This difficulty may be coped with by applying an appropriate regularization procedure in analogy to singular value decomposition in the case of ill-conditioned or underdetermined linear least-squares problems. See [24–26] for an overview on methods for (ill-posed) inverse problems. An adequate quadratic regularization term Q_{reg} to be added to the error function Q with some weighting is in the present context:

$$Q_{\mathrm{reg}} = \frac{1}{2}\left[1 - \frac{1}{L}\sum_{\alpha=1}^{L}\sum_{i=1}^{L}\widehat{P}_{\alpha i}^2 + \frac{1}{L}\sum_{\alpha=L+1}^{S}\sum_{i=1}^{L}\widehat{P}_{\alpha i}^2\right] \tag{69}$$

It measures the deviation of the PIP-space from the subspace of the first L EOFs and takes values between 0 and 1 for sets of patterns satisfying the constraint of Eqs. (52) and (61), respectively. If the PIP-space is identical with the space of the L leading EOFs then $Q_{\mathrm{reg}} = 0$; if it is orthogonal to the L leading EOFs then $Q_{\mathrm{reg}} = 1$. Consider a convex linear combination of Q and Q_{reg}:

$$Q' = \eta Q + (1 - \eta) Q_{\mathrm{reg}}, \quad 0 \leq \eta \leq 1 \tag{70}$$

In the case $\eta = 0$ the solution to the minimization problem is then given by the EOF-model with L modes, which can be stably determined from a finite sample if L is not too large. With increasing value of η more and more information from the variational principle is included. Using several independent data samples the maximum value of η for which the pattern identification is stable can be determined. Hence the EOF-model serves as a kind of minimum standard; an improvement of the patterns, as far as possible on the basis of the available data, is made in a controllable way.

An additional problem is the possible occurrence of several local minima. Because of the nonlinearity of Q there are neither rigorous statements on the existence of local minima nor systematic ways to avoid them in the numerical minimization procedure. Nevertheless with the system considered in this study always only one minimum was found in several minimization procedures starting from different initial pattern sets.

6. Results and discussion

The EOFs of the system have been estimated from a data sample of 50000 points (sampled every third day). Fig. 1 gives an overview on the distribution of variance in the system with respect to the three different metrics. When using the anomaly streamfunction metric the variance is dominated by relatively few low-frequency patterns (red spectrum) with large-scale spatial structure. The turbulent kinetic energy and especially the turbulent enstrophy metric puts more weight on the small scale structures of the flow (higher wavenumbers, higher frequencies). Hence the turbulent kinetic energy and enstrophy are spread out across more patterns.

Minimizations of the error function have been carried out for various numbers of Principal Interaction Patterns and retained EOFs using the three different metrics. They are based on a data sample of 10000 points (sampled every fifth day); i.e. the time average in the variational principle is taken as a time average over this data set. The time derivatives of the model states have been calculated exactly from the spectral model. This turned out to be crucial. If the time derivatives are just estimated from the time series of the states by finite differences they appeared to be quite sensitive to the sampling time interval and not all of the results discussed in the following can be reproduced. In all cases the minimization starts out from the first L EOFs taken as a first guess for the patterns (except for some control runs to check the independence upon the initial pattern set). Best results were obtained using the kinetic energy metric. Hence the study focuses mainly on this case. It turned out to be sufficient to search for the PIPs in a subspace $\mathcal{E}$ of 60 EOFs; no substantial improvement could be obtained by inclusion of higher modes.

6.1. Long-term behaviour

Starting with three patterns and using progressively more modes, 12 PIPs turned out to be the minimum number of degrees of freedom to reproduce the first and second moments in PIP-space quite faithfully. Because of Eqs. (25) and (26) the mean PIP-amplitudes in the full system are zero. A statistically significant deviation of the mean PIP-amplitudes obtained from a long-term integration with the reduced model from zero can be detected, but it is very small. The relative root squared error in the mean state $\sqrt{\langle P\overline{z}, P\overline{z}\rangle / \langle \overline{\Psi}, \overline{\Psi}\rangle}$ is 0.02, the error in the kinetic energy of the mean state is less than 0.3%. Figs. 2a,b give the mean state obtained from an integration with the full model and that obtained from the PIP-model as a contour plot. The accordance is

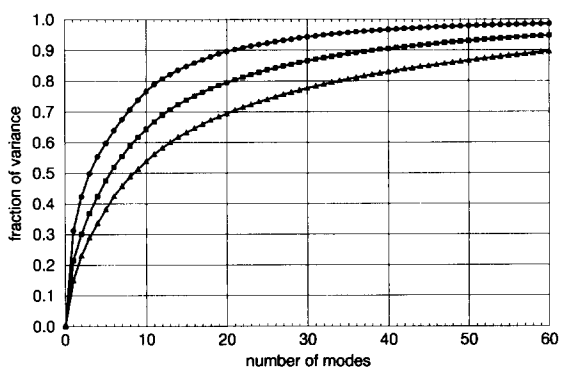

Fig. 1. Fraction of variance captured in an expansion using the first S EOFs with respect to the norm anomaly streamfunction (circles), turbulent kinetic energy (squares) and turbulent enstrophy metric (triangles).

almost perfect. Since the barotropic vorticity equation simulates some aspects of atmospheric flow the plot is superimposed with a map of the northern hemisphere showing the continental outlines.

Long-term integrations of the reduced models show that they tend to have systematically too much variance (and also too much energy and enstrophy). This is due to the fact that the horizontal diffusion term which removes energy from the tail of the spectrum is not captured very well by the PIP- model since it affects mainly the modes of high wavenumbers whereas the PIPs are concentrated on the long and medium waves (large-scale patterns). As demonstrated by Selten in the context of EOF-models [7] this difficulty may be solved by introducing an additional linear damping in the evolution equations for the PIP-amplitudes to parametrize the mean effect of the unresolved modes on the resolved PIP-modes in analogy to the additional diffusion term incorporated in the spectral model. In the present framework this can be done by calculating the elements of B as independent variables according to the variational principle simultaneously with the patterns instead of determining them via Eq. (30). Then one has to solve a system of linear equations resulting from $\frac{\partial Q}{\partial B_{ij}} = 0$ at each step of the optimization with respect to the patterns (see Appendix B). In general, this procedure results in a set of patterns different from that obtained from the minimization in which the matrix B is linked to the patterns via Eq. (30). Fig. 3 shows the energy spectrum obtained from a long- term integration of the full model calculated as

$$\overline{\mathrm{TKE}(n)} = \tfrac{1}{2}n(n+1)\sum_{\alpha|n}\overline{\Psi_\alpha'^2} \tag{71}$$

the energy spectrum of the full model projected onto the PIP-space given by

$$\overline{\mathrm{TKE}^{\mathrm{pip}}(n)} = \tfrac{1}{2}n(n+1)\sum_{\alpha|n}\overline{(PP^{+}\Psi')_\alpha^2} \tag{72}$$

and the energy spectrum obtained from an integration of the PIP-model using 12 modes with additional damping. $\sum_{\alpha|n}$ denotes a sum over all spherical harmonic modes with total wavenumber n. The integration time is taken so long that the errors in the estimation of the second moments are actually negligible. The accordance of the energy spectrum of the PIP-model with the energy spectrum obtained from the projection of the full system onto the PIPs is almost perfect for all wavenumbers; the mean turbulent kinetic energy in PIP- space is 5% too small. Without the damping (not shown) there is only a fair agreement; the mean turbulent kinetic energy is 26% too large. Hence the additional linear damping yields a considerable improvement. Moreover the identification of the elements of B according to the variational principle turns out to be rather well-conditioned; this also may be interpreted as an indication that the parametrization of the influence of the neglected modes onto the resolved modes by an additional damping is adequate in the present situation. From now on only reduced models with additional damping are considered. We now look at the full second-order statistics in PIP-space. Fig. 4 illustrates the mean squared amplitude of the PIP-modes obtained from the reduced model and from a projection of the full model onto these modes. Except for the sixth pattern the accordance is very good. Table 1 gives the correlation matrix of the PIP-amplitudes in the simulation with the reduced model. The standard errors are of the order 10^{-3}. The PIPs are rotated in a way that their amplitudes are uncorrelated in the data of the full system (cf. Eqs. (53) and (62)). Hence the correlation matrix would be the unity matrix in the ideal case. The deviations from zero in the present values are statistically highly significant except for the values indicated as zero. Nevertheless the majority of the values is close to zero. The PIP-model is able to reproduce the second-moment structure in PIP-space quite well.

It was also tried to determine the nonlinear couplings as independent variables from the variational principle rather than from Eq. (29). But this procedure proved not adequate in the present case. The resulting models perform worse than those using the nonlinear couplings from the Galerkin procedure. This is due to the fact

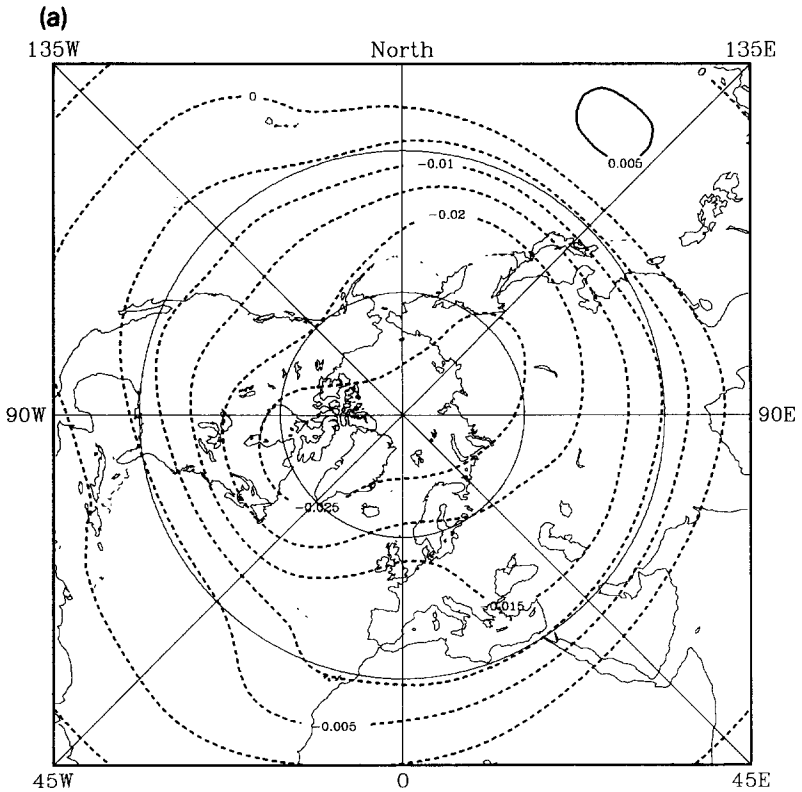

Fig. 2. Mean state obtained from the complete system (a) and from the reduced system using 12 PIPs (b).

Table 1
Correlation matrix of PIP-amplitudes obtained from a long-term simulation with a PIP-model using 12 patterns

	1	2	3	4	5	6	7	8	9	10	11	12
1	1.00	0.07	0.20	0.17	0.00	−0.02	0.32	0.09	−0.05	0.15	0.03	0.03
2		1.00	0.15	0.09	−0.07	−0.02	−0.14	0.22	−0.02	−0.04	−0.11	−0.16
3			1.00	0.04	−0.12	0.06	−0.09	0.02	0.00	−0.02	−0.07	−0.07
4				1.00	0.11	0.09	0.19	0.08	0.00	0.03	0.18	0.05
5					1.00	−0.10	0.03	−0.13	0.15	−0.02	0.18	0.13
6						1.00	−0.06	0.08	−0.17	0.05	0.19	0.10
7							1.00	0.04	−0.03	0.02	0.10	0.05
8								1.00	−0.15	0.00	−0.08	−0.16
9									1.00	0.14	−0.06	0.03
10										1.00	−0.09	0.08
11											1.00	0.12
12												1.00

that the system of linear equations resulting from $\frac{\partial Q}{\partial A_{ijk}} = 0$ becomes extremely ill- conditioned with increasing dimension of the PIP-model and the long-term behaviour of the reduced system is rather sensitive to the interaction coefficients. If there are too many parameters (the number of elements of A grows as L^3, e.g. a 12-dimensional model has already 936 nonlinear couplings) it is not possible any more to identify them reliably by just minimizing the error between the reduced system and the full system in the local map but not taking

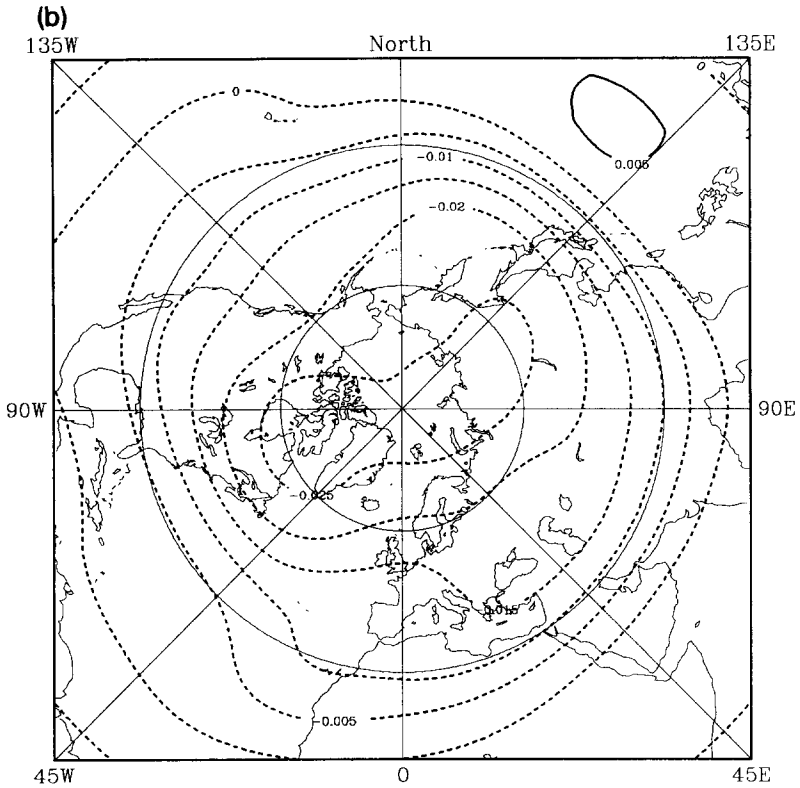

Fig. 2 — continued.

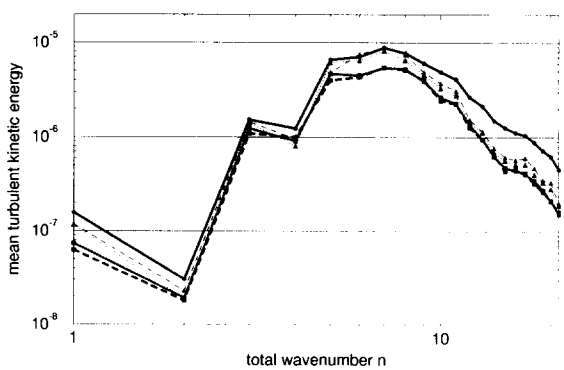

Fig. 3. Energy spectrum of the complete system (thick solid line, circles), of the complete system projected onto the subspace of 12 PIPs (thick dotted line, squares), of the reduced system using 12 PIPs with additional damping (thick dashed line, squares), of the complete system projected onto the subspace of 17 EOFs (thin dotted line, triangles) and of the reduced system using 17 EOFs with additional damping (thin dashed line, triangles).

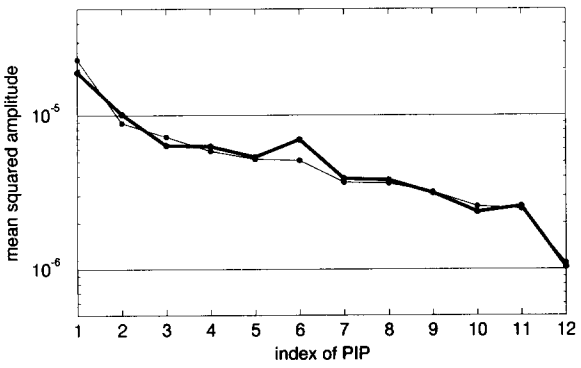

Fig. 4.

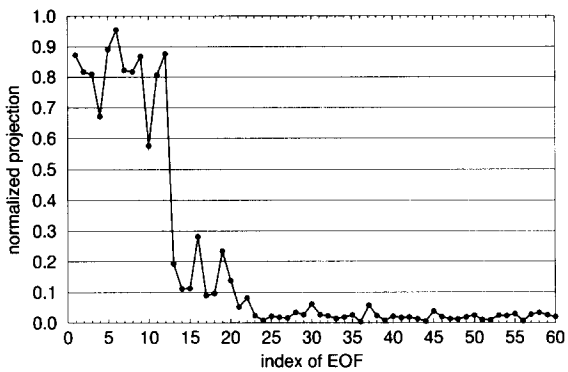

Fig. 5.

Fig. 4. Mean squared PIP-amplitudes obtained from the reduced system with 12 modes (thick line) and from a projection of the complete system onto these modes (thin line).

Fig. 5. Normalized projection of EOFs onto PIP-space.

into account the dynamical behaviour of the reduced model when integrated over a finite time.

If only 11 PIPs are used in the minimization the quality of the model falls off distinctly. The mean state is still reproduced almost perfectly; but the mean turbulent kinetic energy is too low by a factor of about three. If the number of PIPs is increased (calculations have been done up to 15 PIPs) the quality of the dynamical description in the respective PIP-space slowly improves; the PIPs then capture successively more turbulent kinetic energy and hence the PIP-model successively better approximates the full system.

Fig. 3 also shows the energy spectrum obtained from a simulation using 17 EOFs (also with additional damping; otherwise the mean turbulent kinetic energy is 50% too large). The mean state is simulated almost perfectly as with the PIP-model. With truncated models based on EOFs it was not possible to reproduce the energy spectrum with less than 17 modes. In analogy to the PIPs the model drops off sharply when using only 16 EOFs and steadily approaches to the full system when more and more EOFs are included.

To compare the 12-dimensional PIP-space with the space of the leading 12 EOFs the normalized projection $(\sum_i \langle e_\alpha, Mp_i\rangle^2)^{1/2} = (\sum_i \widehat{P}_{\alpha i}^2)^{1/2}$ is given in Fig. 5 for each EOF e_α. The PIP-space is dominated by the leading 12 EOFs but also contains considerable contributions from higher EOFs which are neglected in a 12-dimensional EOF-model and which are responsible for the improvement of the PIP-model on the EOF-model. The sharp decrease between the 12th and 13th EOF is due to the particular regularization procedure. If the EOFs in Eq. (69) would be e.g. weighted by their variance the decrease would be smoother, but the regularization is then less efficient.

Tables 2–5 give information on the spectral composition of the EOFs and the PIPs. For each of the 12 leading EOFs and the 12 PIPs the relative contribution of certain groups of wavenumbers (with respect to the total and zonal wavenumber) to the kinetic energy of the pattern is indicated. The values are rounded to two digits; contributions smaller than 0.005 are indicated as zero. Owing to the orthonormality of the EOFs and PIPs with respect to the kinetic energy metric each row adds up to one (not exactly in all cases due to the rounding). Both the EOF- and the PIP-space are dominated by the long and medium waves. There are only small contributions from the short waves; especially there is hardly any energy in the zonal wavenumbers 11-20. Particularly the first mode (most energetic component) has a large-scale spatial structure (also clearly visible in Figs. 6a and

Table 2
Spectral distribution of the kinetic energy of the EOFs with respect to the total wavenumber

	1–5	6–10	11–15	16–21
1	0.38	0.47	0.11	0.04
2	0.04	0.74	0.17	0.05
3	0.16	0.69	0.10	0.04
4	0.08	0.77	0.10	0.05
5	0.12	0.68	0.13	0.06
6	0.04	0.67	0.23	0.06
7	0.21	0.63	0.11	0.04
8	0.12	0.67	0.16	0.05
9	0.10	0.68	0.18	0.05
10	0.09	0.70	0.16	0.05
11	0.24	0.51	0.16	0.08
12	0.05	0.66	0.23	0.07

Table 3
Spectral distribution of the kinetic energy of the EOFs with respect to the zonal wavenumber

	0–5	6–10	11–15	16–20
1	0.96	0.04	0.00	0.00
2	0.75	0.24	0.01	0.00
3	0.90	0.10	0.01	0.00
4	0.74	0.26	0.00	0.00
5	0.69	0.31	0.00	0.00
6	0.39	0.60	0.01	0.00
7	0.91	0.09	0.00	0.00
8	0.71	0.29	0.01	0.00
9	0.55	0.45	0.00	0.00
10	0.86	0.14	0.01	0.00
11	0.92	0.07	0.00	0.00
12	0.41	0.58	0.01	0.00

Table 4
Spectral distribution of the kinetic energy of the PIPs with respect to the total wavenumber

	1–5	6–10	11–15	16–21
1	0.33	0.49	0.14	0.04
2	0.03	0.73	0.17	0.06
3	0.17	0.64	0.14	0.06
4	0.12	0.69	0.15	0.04
5	0.03	0.70	0.20	0.07
6	0.16	0.63	0.17	0.05
7	0.10	0.75	0.11	0.05
8	0.33	0.54	0.10	0.04
9	0.10	0.64	0.20	0.06
10	0.21	0.47	0.25	0.08
11	0.08	0.61	0.23	0.07
12	0.26	0.42	0.23	0.10

Table 5
Spectral distribution of the kinetic energy of the PIPs with respect to the zonal wavenumber

	0–5	6–10	11–15	16–20
1	0.94	0.06	0.00	0.00
2	0.67	0.32	0.01	0.00
3	0.87	0.12	0.00	0.00
4	0.88	0.12	0.00	0.00
5	0.37	0.63	0.01	0.00
6	0.63	0.36	0.01	0.00
7	0.83	0.17	0.01	0.00
8	0.84	0.15	0.00	0.00
9	0.42	0.57	0.01	0.00
10	0.83	0.17	0.00	0.00
11	0.41	0.58	0.01	0.00
12	0.86	0.12	0.01	0.00

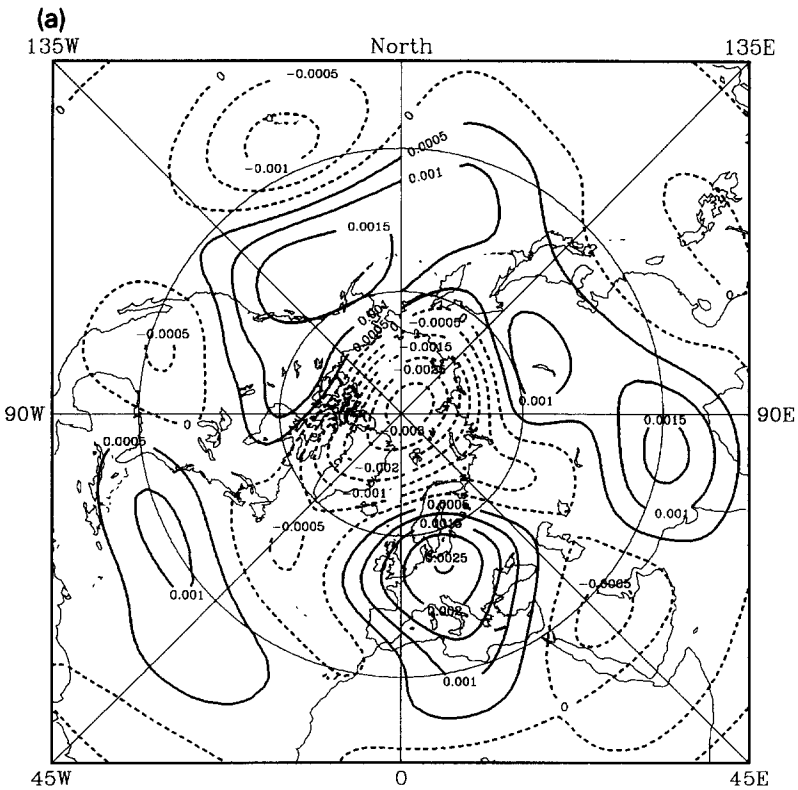

Fig. 6. First (a) and second (b) EOF.

7a); going to the higher modes there is a certain trend towards smaller spatial scales (associated with higher frequencies) with both EOFs and PIPs although not strictly.

Figs. 6a,b and 7a,b show the spatial structure of the two leading EOFs and PIPs, respectively, as isoline plots. The amplitudes of the patterns are set to their standard deviation as occurring in the full model. Hence together with the plot of the mean state (Fig. 2a) Figs. 6 and 7 provide an impression of the nature of the flow. The

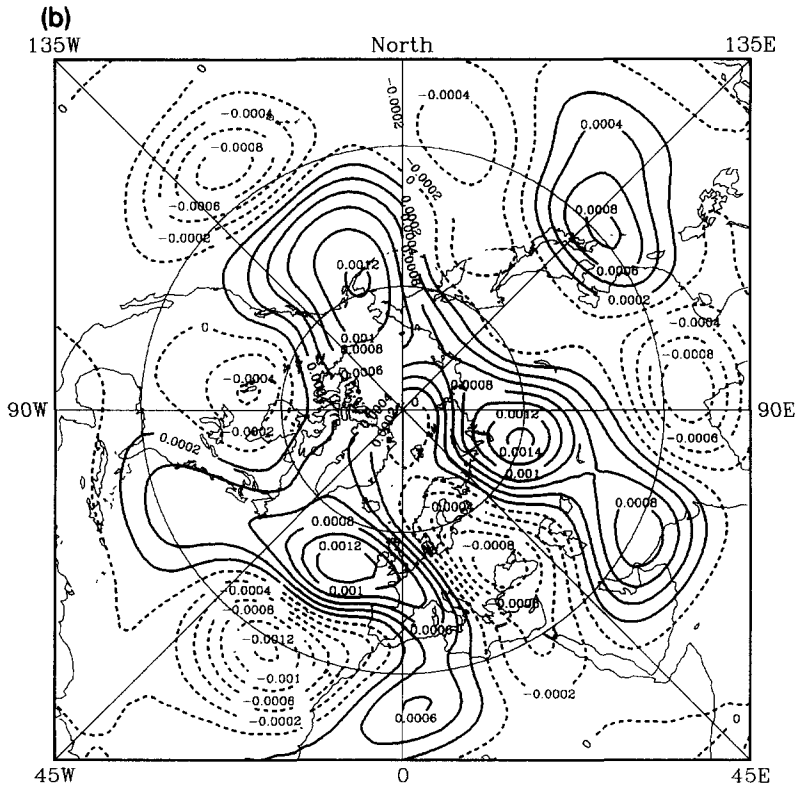

Fig. 6 — continued.

two leading PIPs are quite similar to the corresponding EOFs (especially the first PIP to the first EOF). When looking at higher modes (not shown) differences are more clearly visible.

The fraction of the mean turbulent kinetic energy ($\overline{\mathrm{TKE}^{\mathrm{pip}}}/\overline{\mathrm{TKE}}$) captured by the 12 PIP-modes is 59.4%; the first 12 EOFs contain 69.0%, the first 17 EOFs 76.4%. But the PIP-model still reproduces the essentials of the large-scale pattern evolution.

If the turbulent enstrophy metric $M_3 = \Delta^2$ is used in the projection the same minimum numbers of modes to reproduce the mean and the covariance structure of the amplitudes (12 PIPs, 17 EOFs) were found. But the fraction of energy and enstrophy captured by these 12 PIPs is smaller than in the case of $M_2 = -\Delta$. With the norm anomaly streamfunction metric $M_1 = 1$ the minimum reduced model has to include 15 PIPs and 19 EOFs, respectively. This higher number may be due to the fact that the nonlinear terms in this case have no conserved quantity (cf. Section 4.4).

To demonstrate the efficiency of PIP- and EOF-models compared to models based on spherical harmonics Fig. 8 shows the turbulent kinetic energy spectrum obtained from long-term integrations of spectral models truncated at total wavenumber $n_{\max} = 20$ (210 modes), $n_{\max} = 19$ (190 modes), $n_{\max} = 12$ (78 modes) and $n_{\max} = 5$ (15 modes), respectively, and of the full model ($n_{\max} = 21$, 231 modes). All integrations use the mean state of the full model, only the anomalies are truncated as with the PIP-models to allow for a direct comparison. For this reason the results presented here differ from those obtained by Selten [7]; in the latter study a spectral model truncated at wavenumber $n_{\max} = 20$ performs worse than is reported here since the mean state is truncated, too. Already with a model truncated at wavenumber $n_{\max} = 19$ the error in the energy spectrum is as large as with the PIP-model (Fig. 3) although the number of modes involved in the spectral

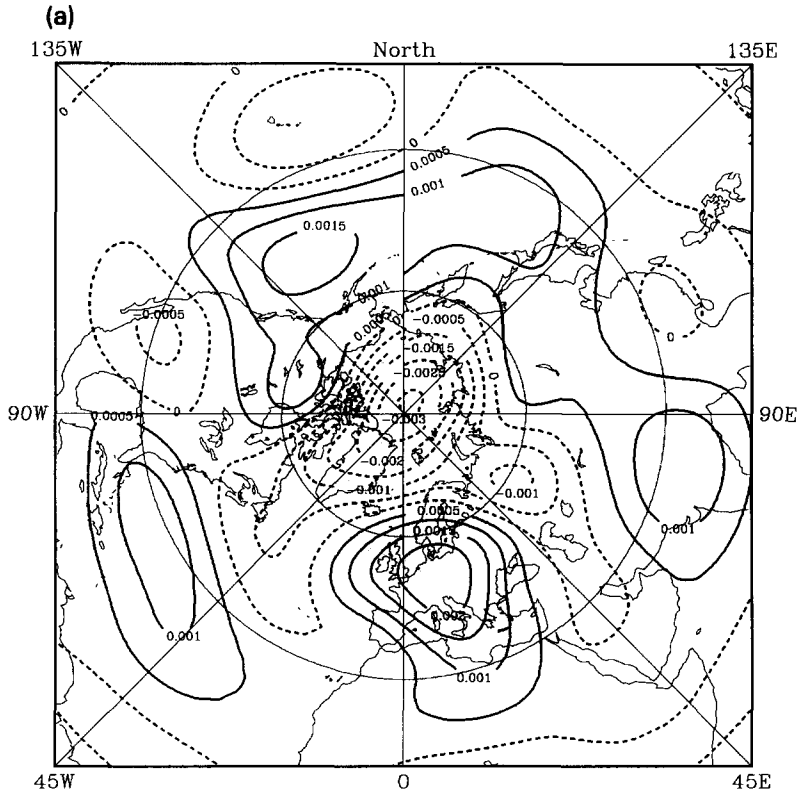

Fig. 7. First (a) and second (b) PIP.

model is by an order of magnitude higher; with the spectral model truncated at wavenumber $n_{\max} = 12$ the error is considerably larger and the spectral model truncated at wavenumber $n_{\max} = 5$ which has a number of degrees of freedom comparable to that of the PIP- and EOF-models completely fails to capture the energy spectrum. In analogy with the PIP- and EOF-models new damping rates for all spherical harmonic modes were determined according to the same variational principle; but no substantial improvement could be obtained by this procedure for spectral models in accordance with the finding of Selten [7]. This clearly demonstrates that PIP- and EOF-models are far more efficient than spectral models as to the number of modes required.

6.2. *Local properties*

Fig. 9 shows the correlation between the tendencies of the PIP-amplitudes given by the truncated model and those given by the full model separately for each pattern:

$$\mathrm{cor}_i = \frac{\mathrm{Cov}(\dot{z}_i^{\mathrm{pip}}, \dot{z}_i)}{\sqrt{\mathrm{Var}(\dot{z}_i^{\mathrm{pip}})}\sqrt{\mathrm{Var}(\dot{z}_i)}}, \quad i = 1, \cdots, L \tag{73}$$

with

$$\mathrm{Cov}(a, b) = \overline{ab} - \overline{a}\,\overline{b}, \tag{74}$$

$$\mathrm{Var}(a) = \overline{a^2} - \overline{a}^2 \tag{75}$$

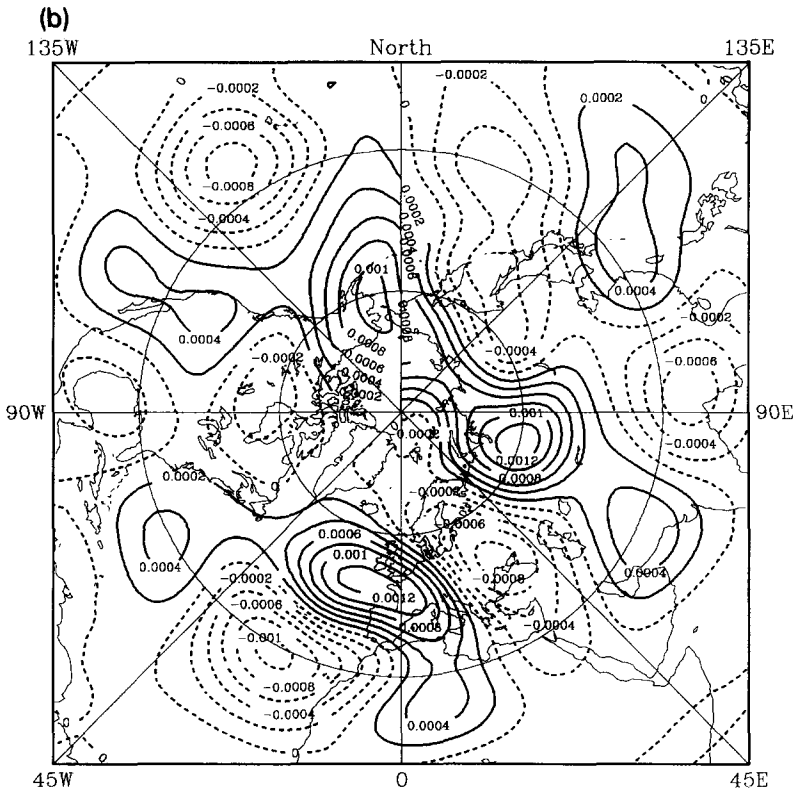

Fig. 7 — continued.

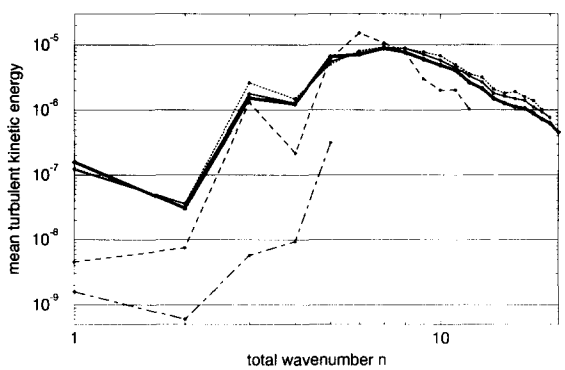

Fig. 8. Energy spectrum of spectral models truncated at wavenumber 21 (complete system, thick solid line), wavenumber 20 (thin solid line), wavenumber 19 (dotted line), wavenumber 12 (dashed line) and wavenumber 5 (dotted-dashed line).

It also gives the explained tendency variance for each pattern defined by:

$$s_i = 1 - \frac{\mathrm{Var}(\dot{z}_i^{\mathrm{pip}} - \dot{z}_i)}{\mathrm{Var}(\dot{z}_i)}, \quad i = 1, \cdots, L \tag{76}$$

The quantities are estimated from a data sample of 50000 points (sampled every third day) different from the sample used for the minimization. Both $\overline{\dot{z}_i^{\mathrm{pip}}}$ and $\overline{\dot{z}_i}$ do not deviate from zero statistically significant for all

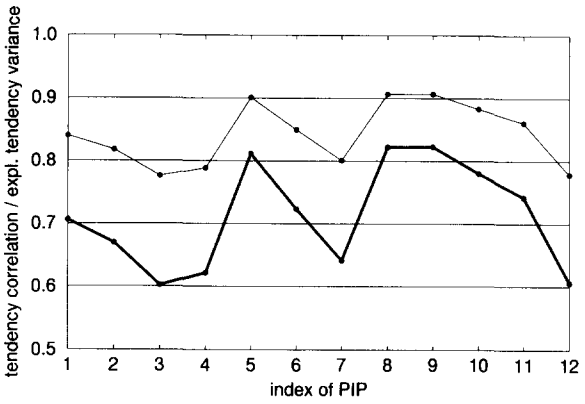

Fig. 9.

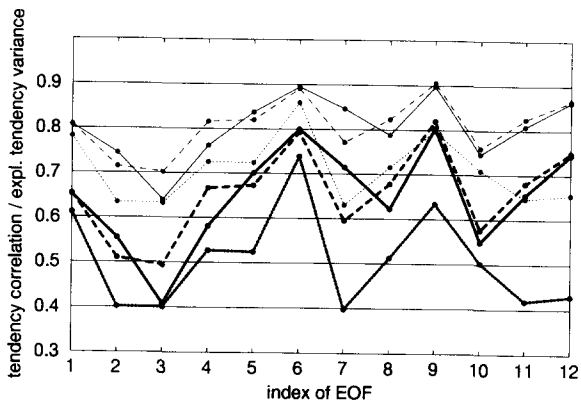

Fig. 10.

Fig. 9. Tendency correlation (thin line) and explained tendency variance (thick line) of PIP-amplitudes for the reduced model using 12 PIPs.

Fig. 10. Tendency correlation (thin lines) and explained tendency variance (thick lines) of EOF-amplitudes for reduced models using 12 EOFs (dotted), 17 EOFs (dashed) and 12 PIPs (solid).

patterns. The standard errors of the estimates of cor_i and s_i are of the order 10^{-3} and are therefore not indicated in detail. For all PIP-modes a very large part of the tendency variance is explained by the reduced model.

The corresponding values for the first 12 EOFs are in Fig. 10. The PIP-model provides a considerable improvement on the EOF-model; even the tendencies of the EOFs are captured better by the PIP-model than by the EOF-model. About 17 EOFs are necessary to describe the tendencies of the first 12 EOFs as well as with 12 PIPs.

6.3. Prediction experiments

Now the ability of the truncated model to predict the time evolution of the PIP-amplitudes for a finite time is investigated. Starting out from an initial anomaly field $\Psi'(0)$ the PIP-model is integrated in time with the initial condition $z(0) = P^+\Psi'(0)$. The quality of the forecasts as a function of the prediction time τ is measured by the mean anomaly correlation

$$\{\mathrm{Acor}(\tau)\} = \left\{ \frac{\langle \Psi'^{\mathrm{pip}}(\tau), \Psi'^{\mathrm{pred}}(\tau) \rangle}{\sqrt{\langle \Psi'^{\mathrm{pip}}(\tau), \Psi'^{\mathrm{pip}}(\tau) \rangle} \sqrt{\langle \Psi'^{\mathrm{pred}}(\tau), \Psi'^{\mathrm{pred}}(\tau) \rangle}} \right\} \tag{77}$$

and the relative root mean squared error

$$\mathrm{rrmse}(\tau) = \sqrt{\frac{\{\langle \Psi'^{\mathrm{pip}}(\tau) - \Psi'^{\mathrm{pred}}(\tau), \Psi'^{\mathrm{pip}}(\tau) - \Psi'^{\mathrm{pred}}(\tau) \rangle\}}{\{\langle \Psi'^{\mathrm{pip}}(\tau), \Psi'^{\mathrm{pip}}(\tau) \rangle\}}} \tag{78}$$

$\Psi'^{\mathrm{pip}}(\tau) = PP^+\Psi'(\tau)$ is the anomaly field at time τ given by the full model projected onto PIP-space; $\Psi'^{\mathrm{pred}}(\tau) = Pz(\tau)$ is the field predicted by the PIP-model. The braces denote an average over the ensemble of forecasts, here 2000 uncorrelated forecasts. The forecast periods are different from the data sample used to determine the PIPs. For comparison the skill of spectral models truncated at wavenumber 20 (210 modes), wavenumber 18 (171 modes) and wavenumber 16 (136 modes) is indicated, too. The persistence forecast

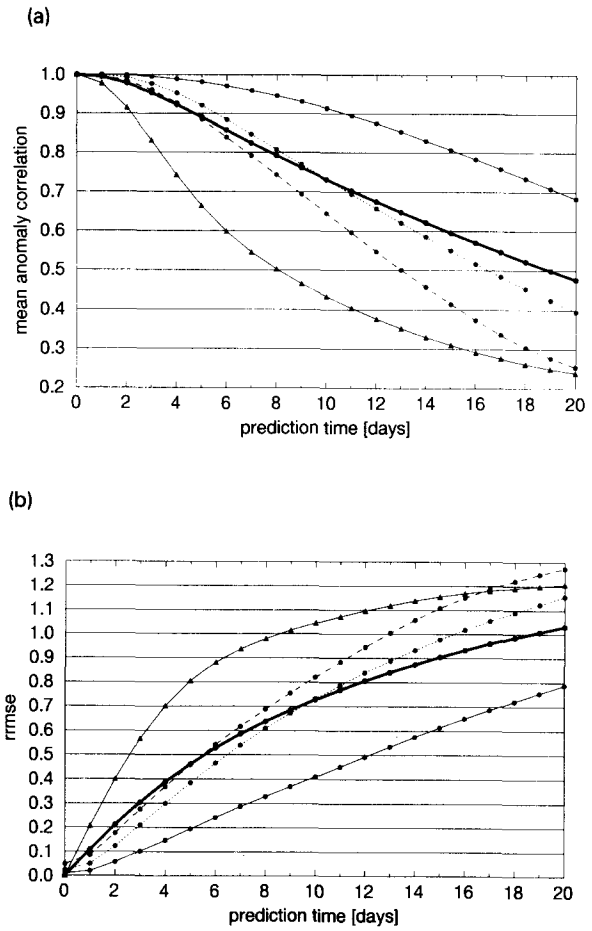

Fig. 11. Skill of the PIP-model using 12 modes (thick solid line) and of spectral models truncated at wavenumber 20 (thin solid line, circles), wavenumber 18 (dotted line) and wavenumber 16 (dashed line) in predicting the PIP-amplitudes measured by the mean anomaly correlation (a) and by the relative root mean squared error (b) as a function of prediction time. The persistence is indicated as a control forecast (thin solid line, triangles).

$\Psi'^{\mathrm{pers}}(\tau) = \Psi'^{\mathrm{pip}}(0)$ simply reflecting the autocorrelation of the PIP-amplitudes is considered as a trivial control forecast. Note that the reference integration of the full model starts from the full initial condition $\Psi'(0)$. Figs. 11a,b show the results. The PIP-forecasts using 12 patterns have considerable skill. The skill of the spectral models rapidly falls off with decreasing truncation limit. Again there is some difference to the results reported by Selten [7] concerning the spectral model truncated at wavenumber 20 for the reason already mentioned above.

The errors in the prediction experiments consist of two parts: The first part comes from the truncation error of the reduced system. Moreover the projection onto the PIPs causes an error in the initial condition which leads to prediction errors due to the inherent instability present in the full system. To investigate the influence of the truncation error alone further prediction experiments have been performed starting from initial conditions $PP^{+}\Psi'(0)$ lying in PIP-space instead of $\Psi'(0)$. Hence now the PIP-model and the reference integration with the full model start from the same initial condition. The forecast skill is now much better (Figs. 12a,b). This indicates that a large part of the errors of the PIP-model in Figs. 11a,b is due to the error in the initial condition.

Last the ability of the reduced models to predict the time evolution of the most energetic components is

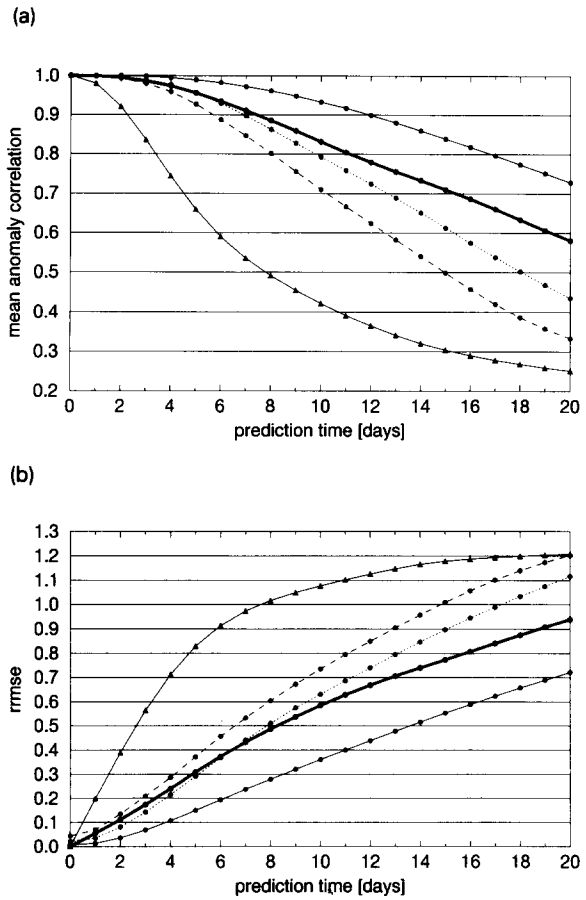

Fig. 12. Same as Fig. 11, but with initial conditions projected onto PIP-space.

investigated. Figs. 13a,b refer to the same prediction experiments as Figs. 11a,b, but now the skill concerning the amplitudes of the first 12 EOFs instead of the PIPs is evaluated. The PIP- model starts with an error at the beginning since the EOFs are not fully contained in PIP-space. But after some time the predictions with the PIP-model are better than those with the EOF-model because the dynamics are captured better by the PIP-model.

7. Conclusions

An algorithm for constructing optimal low-dimensional models of complex dynamical systems has been described. An optimal linear subspace spanned by a few characteristic spatial patterns and the coefficients of a dynamical system describing the time evolution of these modes are determined simultaneously according to a variational principle. The method involves higher-order correlation tensors of the variables as well as their time derivatives and leads to a nonlinear minimization problem in contrast to e.g. EOF-analysis which is based on second-order statistics and leads to an eigenvalue problem. In an application to a two- dimensional fluid system the leading EOFs turn out to be already a rather good approximation to the optimal modes, but the PIPs provide a considerable improvement, a PIP-model with 12 modes being approximately as good as an EOF-model with

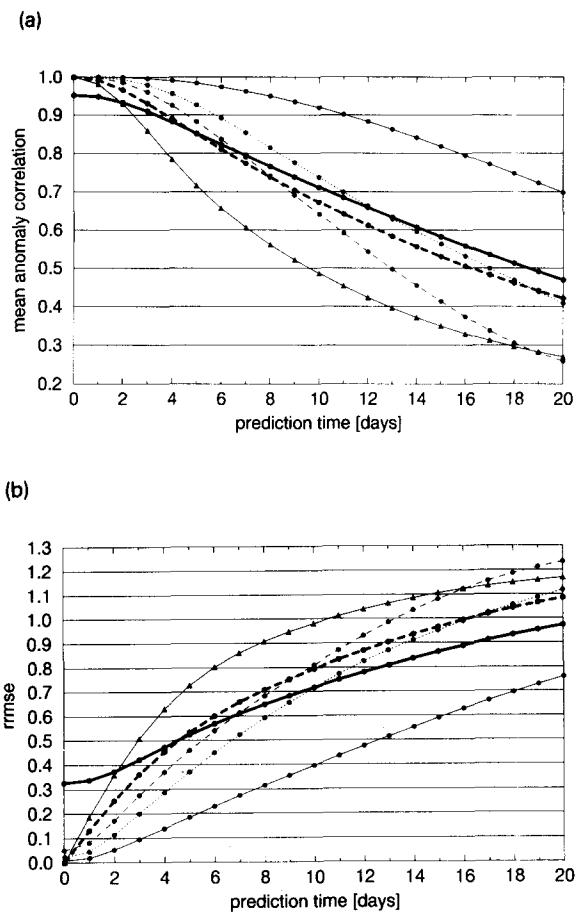

Fig. 13. Skill of a reduced model using 12 EOFs (thick dashed line), a reduced model using 12 PIPs (thick solid line) and of spectral models truncated at wavenumber 20 (thin solid line, circles), wavenumber 18 (dotted line) and wavenumber 16 (thin dashed line) in predicting the amplitudes of the first 12 EOFs measured by the mean anomaly correlation (a) and the relative root mean squared error (b) as a function of prediction time. The persistence is indicated as a control forecast (thin solid line, triangles).

17 patterns as to both global behaviour monitored by second-order statistics and short time prediction skill. Both PIP- and EOF-models are far more efficient than models based on spherical harmonics.

The original PIP reduction as outlined in Section 2 has been modified in this study in two ways. First, for computational tractability the minimization procedure is carried out in the space spanned by a certain number of leading EOFs rather than in the full spectral space. The latter is impracticable in the present case. A reduction in the full spectral space may be adequate for systems requiring a lower number of modes in the Fourier expansion, e.g. systems close to bifurcation points. Secondly, in the original PIP reduction the dynamic equations of the reduced model are specified within a model class involving arbitrary parameters to be determined in the minimization procedure simultaneously with the patterns whereas in the present study the model parameters (at least the nonlinear couplings) are obtained by a projection procedure. For the system under consideration here it turned out not to be useful to infer the nonlinear couplings from the data. The parameter identification is ill-posed and thus the algorithm is not capable of extracting the parameters reliably if there are too many. The resulting reduced models then perform worse than the models discussed in Section 6 using the nonlinear couplings obtained from the Galerkin projection. Presumably, the complete calculation of

the parameters in a nonlinear model directly from the time series is only suitable for systems exhibiting very low-dimensional behaviour which thus can be described using only very few modes and for which the model class can be restricted (by a priori knowledge or assumptions about the system) to only a few adjustable parameters (cf. [9–12]).

Acknowledgements

Part of this work was prepared during a visit to the Royal Netherlands Meteorological Institute. I would like to thank F. Selten for providing the computer code of the barotropic spectral model and for helpful discussions. Moreover the comments of three anonymous reviewers helped to improve the content and the clarity of the paper.

Appendix A. Minimization of the error function

The numerical minimization is performed using a Quasi-Newton algorithm with BFGS-update. The constraints are treated with Lagrangian multipliers. The method requires exact evaluation of the error function Q, the constraints and the regularization term Q_{reg} as well as their gradients for arbitrary sets of patterns. See [27,28] for some background on the theory and implementation of Quasi-Newton methods.

In the following greek indices always run from 1 to S, latin ones from 1 to L. Introducing the error of the PIP-model in the time derivative of the PIP-modes

$$\varepsilon_i\left(z(\widehat{P}),\dot{z}(\widehat{P}),A(\widehat{P}),B(\widehat{P}),C(\widehat{P})\right)=\dot{z}_i^{\mathrm{pip}}-\dot{z}_i=\tfrac{1}{2}\sum_{j,k}A_{ijk}z_jz_k+\sum_j B_{ij}z_j+C_i-\dot{z}_i \tag{79}$$

the error function Q of Eq. (60) and its derivatives are most efficiently evaluated by expressing them in terms of moments of the error ε, the PIP- and EOF-coefficients z and $\widehat{\Psi}$ and their time derivatives $\dot{z}$ and $\dot{\widehat{\Psi}}$. In fact the minimization procedure refers to the PIPs represented in the basis E° instead of E as remarked in Section 5.3. Hence Q, Q_{reg} and the constraints of Eqs. (61) and (62) have to be expressed as functions of $\widehat{P}^\circ$ rather than $\widehat{P}$ involving the transformed quantities $\widehat{P}^{\circ+}$, $\widehat{\Gamma}^\circ$, $\widehat{\Pi}^\circ$, $\widehat{\Psi}^\circ$ and $\dot{\widehat{\Psi}}^\circ$, but the circles are dropped here to facilitate the notation.

$$Q\left(\widehat{P}\right)=Q\left(\widetilde{M}(\widehat{P}),z(\widehat{P}),\dot{z}(\widehat{P}),A(\widehat{P}),B(\widehat{P}),C(\widehat{P})\right)=\sum_{i,j}\widetilde{M}_{ij}\,\overline{\varepsilon_i\varepsilon_j} \tag{80}$$

The variation of Q with respect to the patterns $\widehat{p}_i$ and the parameters A, B and C yields:

$$\begin{aligned}\frac{\partial Q}{\partial\widehat{P}_{\alpha r}}&=\sum_{i,j}\frac{\partial Q}{\partial\widetilde{M}_{ij}}\frac{\partial\widetilde{M}_{ij}}{\partial\widehat{P}_{\alpha r}}+\sum_i\left(\frac{\partial Q}{\partial z_i}\frac{\partial z_i}{\partial\widehat{P}_{\alpha r}}+\frac{\partial Q}{\partial\dot{z}_i}\frac{\partial\dot{z}_i}{\partial\widehat{P}_{\alpha r}}\right)\\&=\sum_{i,j}\frac{\partial\widetilde{M}_{ij}}{\partial\widehat{P}_{\alpha r}}\overline{\varepsilon_i\varepsilon_j}+2\sum_{i,j}\widetilde{M}_{ij}\,\overline{\frac{\partial\varepsilon_i}{\partial\widehat{P}_{\alpha r}}\varepsilon_j}\\&=\sum_{i,j}\frac{\partial\widetilde{M}_{ij}}{\partial\widehat{P}_{\alpha r}}\overline{\varepsilon_i\varepsilon_j}+2\sum_{i,j}\widetilde{M}_{ij}\left[\sum_{k,l}A_{ikl}\left(D^{-1}_{kr}\,\overline{\varepsilon_jz_lw_\alpha}-\widehat{P}^{+}_{k\alpha}\,\overline{\varepsilon_jz_lz_r}\right)\right.\end{aligned}$$

$$+ \sum_k B_{ik} \left(D_{kr}^{-1} \overline{\varepsilon_j w_\alpha} - \widehat{P}_{k\alpha}^{+} \overline{\varepsilon_j z_r} \right) - \left(D_{ir}^{-1} \overline{\varepsilon_j \dot{w}_\alpha} - \widehat{P}_{i\alpha}^{+} \overline{\varepsilon_j \dot{z}_r} \right) \Bigg] \tag{81}$$

with

$$\frac{\partial \widetilde{M}_{ij}}{\partial \widehat{P}_{\alpha r}} = \sum_{k,l} \Bigg(V_{kl}^{-1} \left[\left(\delta_{jr} \widehat{P}_{\alpha l} + \delta_{lr} \widehat{P}_{\alpha j} \right) D_{ik} + \left(\delta_{ir} \widehat{P}_{\alpha k} + \delta_{kr} \widehat{P}_{\alpha i} \right) D_{jl} \right]$$

$$- D_{ik} D_{jl} \widehat{\Pi}_{\alpha\alpha} \sum_m \widehat{P}_{\alpha m} \left(V_{km}^{-1} V_{lr}^{-1} + V_{kr}^{-1} V_{lm}^{-1} \right) \Bigg) , \tag{82}$$

$$D = \widehat{P}^t \widehat{P} , \tag{83}$$

$$V = \widehat{P}^t \widehat{\Pi} \widehat{P} , \tag{84}$$

$$\frac{\partial \varepsilon_i}{\partial \widehat{P}_{\alpha r}} = \sum_j \left(\frac{\partial \varepsilon_i}{\partial z_j} \frac{\partial z_j}{\partial \widehat{P}_{\alpha r}} + \frac{\partial \varepsilon_i}{\partial \dot{z}_j} \frac{\partial \dot{z}_j}{\partial \widehat{P}_{\alpha r}} \right) = \sum_{j,k} A_{ijk} \frac{\partial z_j}{\partial \widehat{P}_{\alpha r}} z_k + \sum_j B_{ij} \frac{\partial z_j}{\partial \widehat{P}_{\alpha r}} - \frac{\partial \dot{z}_i}{\partial \widehat{P}_{\alpha r}} , \tag{85}$$

$$\frac{\partial z_i}{\partial \widehat{P}_{\alpha r}} = D_{ir}^{-1} w_\alpha - \widehat{P}_{i\alpha}^{+} z_r , \tag{86}$$

$$\frac{\partial \dot{z}_i}{\partial \widehat{P}_{\alpha r}} = D_{ir}^{-1} \dot{w}_\alpha - \widehat{P}_{i\alpha}^{+} \dot{z}_r , \tag{87}$$

$$w_\alpha = \widehat{\Psi}_\alpha - \sum_i \widehat{P}_{\alpha i} z_i , \tag{88}$$

$$\dot{w}_\alpha = \widehat{\dot{\Psi}}_\alpha - \sum_i \widehat{P}_{\alpha i} \dot{z}_i \tag{89}$$

Without loss of generality $\widehat{\Pi}$ is assumed to be diagonal in formula (82) (cf. Section 5.3)

$$\frac{\partial Q}{\partial A_{ijk}} = \sum_l \widetilde{M}_{il} \overline{\varepsilon_l z_j z_k} , \tag{90}$$

$$\frac{\partial Q}{\partial B_{ij}} = 2 \sum_l \widetilde{M}_{il} \overline{\varepsilon_l z_j} , \tag{91}$$

$$\frac{\partial Q}{\partial C_i} = 2 \sum_l \widetilde{M}_{il} \overline{\varepsilon_l} \tag{92}$$

The total derivative with respect to the patterns reads:

$$\frac{dQ}{d\widehat{P}_{\alpha r}} = \frac{\partial Q}{\partial \widehat{P}_{\alpha r}} + \sum_{i,j,k} \frac{\partial Q}{\partial A_{ijk}} \frac{\partial A_{ijk}}{\partial \widehat{P}_{\alpha r}} + \sum_{i,j} \frac{\partial Q}{\partial B_{ij}} \frac{\partial B_{ij}}{\partial \widehat{P}_{\alpha r}} + \sum_i \frac{\partial Q}{\partial C_i} \frac{\partial C_i}{\partial \widehat{P}_{\alpha r}} \tag{93}$$

The derivatives of the interaction tensors with respect to the patterns occurring in Eq. (93) are given in Appendix C.

Appendix B. Calculation of interaction coefficients

There are basically two possibilities to evaluate the tensors of interaction coefficients of a reduced model. On the one hand one can consider the PIPs in the full phase space of spherical harmonics and calculate the coefficients according to formulae (29)–(31) using the transform method. The computational effort is dominated by the calculation of P and P^* from $\widehat{P}$ and $\widehat{P}^*$ according to $P = E\widehat{P}$ and $P^* = E\widehat{P}^*$ ($\mathcal{O}(LSN)$ operations), the evaluation of the Jacobian terms in Eq. (29) ($\mathcal{O}(L^2N^{3/2})$ operations) and the projection of the Jacobians onto the adjoint patterns ($\mathcal{O}(L^3N)$ operations). On the other hand it is possible to take advantage of the fact that the PIPs lie in the subspace $\mathcal{E}$ of retained EOFs and then to proceed as follows. The tensors of coefficients $A^{\text{eof}}, B^{\text{eof}}$ and C^{eof} of the reduced model using the leading S EOFs as basis functions ($p_i = e_i, L = S$) are calculated once explicitly according to formulae (29)–(31) using the transform method:

$$A^{\text{eof}}_{\alpha\beta\gamma} = -\langle e_\alpha, M\Delta^{-1}\left[\mathcal{J}(e_\beta, \Delta e_\gamma) + \mathcal{J}(e_\gamma, \Delta e_\beta)\right]\rangle\,, \tag{94}$$

$$B^{\text{eof}}_{\alpha\beta} = -\langle e_\alpha, M\left(\Delta^{-1}\left[\mathcal{J}(\overline{\Psi}, \Delta e_\beta) + \mathcal{J}(e_\beta, \Delta\overline{\Psi} + f + h)\right] + \kappa_1 e_\beta + \kappa_2\Delta^3 e_\beta\right)\rangle\,, \tag{95}$$

$$C^{\text{eof}}_{\alpha} = \langle e_\alpha, M\left(\widetilde{\Psi} - \Delta^{-1}\mathcal{J}(\overline{\Psi}, \Delta\overline{\Psi} + f + h) - \kappa_1\overline{\Psi} - \kappa_2\Delta^3\overline{\Psi}\right)\rangle \tag{96}$$

Here $e^*_\alpha = e_\alpha$ holds because of $e^t_\alpha M e_\beta = \delta_{\alpha\beta}$. In the actual calculations the rotated patterns e°_α introduced in Section 5.3 are used instead of e_α, but the circles are dropped now for convenience of notation. The coefficients of the PIP-model are then calculated by direct summation in the S-dimensional EOF-space using the identities

$$A_{ijk} = \sum_{\alpha,\beta,\gamma} \widehat{P}^+_{i\alpha}\widehat{P}_{\beta j}\widehat{P}_{\gamma k}A^{\text{eof}}_{\alpha\beta\gamma}\,, \tag{97}$$

$$B_{ij} = \sum_{\alpha,\beta} \widehat{P}^+_{i\alpha}\widehat{P}_{\beta j}B^{\text{eof}}_{\alpha\beta}\,, \tag{98}$$

$$C_i = \sum_{\alpha} \widehat{P}^+_{i\alpha}C^{\text{eof}}_{\alpha} \tag{99}$$

involving $\mathcal{O}(LS^3)$ operations. Hence the latter method is preferable for small S, the former one for large S. The turning point is about $S \approx 40$ (with $L = 12$). When S approaches to N the calculation in spherical harmonic space is far more efficient.

If the matrix B of linear interaction coefficients is determined from the variational principle rather than from the dynamic equation (cf. Section 6.1) one has to solve a positive definite system of L^2 linear equations resulting from $\frac{\partial Q}{\partial B_{ij}} = 0$. In this equations the metric can be removed; the system then takes a block-diagonal structure and each row of B can be obtained separately from a positive definite linear system of dimension L:

$$\sum_j W_{jk}B_{ij} = y^i_k \tag{100}$$

with

$$W_{jk} = \overline{z_j z_k}\,, \tag{101}$$

$$y^i_k = \overline{\dot{z}_i z_k} - \overline{q_i z_k} - C_i\,\overline{z_k}\,, \tag{102}$$

$$q_i = \tfrac{1}{2}\sum_{j,k} A_{ijk}z_j z_k \tag{103}$$

Note that the system matrix W is independent of i. Hence its Cholesky decomposition has to be computed only once for a given set of patterns; then all elements of B are obtained by backsubstitution.

Appendix C. Derivative of interaction coefficients

The first order variation of the coefficients of the PIP-model with respect to the patterns yields:

$$\frac{\partial A_{ijk}}{\partial \widehat{P}_{\alpha r}} = D^{-1}_{ir}\left(\Lambda_{\alpha jk} - \sum_l \widehat{P}_{\alpha l} A_{ljk}\right) - \widehat{P}^{+}_{i\alpha} A_{rjk} + \delta_{jr}\,\Theta_{ik\alpha} + \delta_{kr}\,\Theta_{ij\alpha}\,, \tag{104}$$

$$\frac{\partial B_{ij}}{\partial \widehat{P}_{\alpha r}} = D^{-1}_{ir}\left(\Upsilon_{\alpha j} - \sum_l \widehat{P}_{\alpha l} B_{lj}\right) - \widehat{P}^{+}_{i\alpha} B_{rj} + \delta_{jr}\,\Xi_{i\alpha}\,, \tag{105}$$

$$\frac{\partial C_i}{\partial \widehat{P}_{\alpha r}} = D^{-1}_{ir}\left(X_\alpha - \sum_l \widehat{P}_{\alpha l} C_l\right) - \widehat{P}^{+}_{i\alpha} C_r \tag{106}$$

with the tensors

$$\Lambda_{\alpha jk} = -\langle e_\alpha, M\Delta^{-1}\left[\mathcal{J}(p_j,\Delta p_k) + \mathcal{J}(p_k,\Delta p_j)\right]\rangle\,, \tag{107}$$

$$\Theta_{ij\alpha} = -\langle p^*_i, M\Delta^{-1}\left[\mathcal{J}(e_\alpha,\Delta p_j) + \mathcal{J}(p_j,\Delta e_\alpha)\right]\rangle\,, \tag{108}$$

$$\Upsilon_{\alpha j} = -\langle e_\alpha, M\left(\Delta^{-1}\left[\mathcal{J}(\overline{\Psi},\Delta p_j) + \mathcal{J}(p_j,\Delta\overline{\Psi} + f + h)\right] + \kappa_1 p_j + \kappa_2\Delta^3 p_j\right)\rangle\,, \tag{109}$$

$$\Xi_{i\alpha} = -\langle p^*_i, M\left(\Delta^{-1}\left[\mathcal{J}(\overline{\Psi},\Delta e_\alpha) + \mathcal{J}(e_\alpha,\Delta\overline{\Psi} + f + h)\right] + \kappa_1 e_\alpha + \kappa_2\Delta^3 e_\alpha\right)\rangle\,, \tag{110}$$

$$X_\alpha = \langle e_\alpha, M\left(\widetilde{\Psi} - \Delta^{-1}\mathcal{J}(\overline{\Psi},\Delta\overline{\Psi} + f + h) - \kappa_1\overline{\Psi} - \kappa_2\Delta^3\overline{\Psi}\right)\rangle \tag{111}$$

As with the coefficients themselves there exist two ways of calculating the derivatives numerically. On the one hand again one can calculate the required tensors according to the formulae (107)–(111) in the basis of spherical harmonics using the transform method requiring in leading order $\mathcal{O}(LSN^{3/2})$ and $\mathcal{O}(L^2SN)$ operations (for the calculation and projection of the Jacobian terms in Θ and Λ). The other possibility is direct summation in EOF-space using the identities

$$\Lambda_{\alpha jk} = \sum_{\beta,\gamma} \widehat{P}_{\beta j}\widehat{P}_{\gamma k} A^{\mathrm{eof}}_{\alpha\beta\gamma}\,, \tag{112}$$

$$\Theta_{ij\alpha} = \sum_{\beta,\gamma} \widehat{P}^{+}_{i\beta}\widehat{P}_{\gamma j} A^{\mathrm{eof}}_{\beta\alpha\gamma}\,, \tag{113}$$

$$\Upsilon_{\alpha j} = \sum_{\beta} \widehat{P}_{\beta j} B^{\mathrm{eof}}_{\alpha\beta}\,, \tag{114}$$

$$\Xi_{i\alpha} = \sum_{\beta} \widehat{P}^{+}_{i\beta} B^{\mathrm{eof}}_{\beta\alpha} \tag{115}$$

$$X_\alpha = C^{\mathrm{eof}}_\alpha \tag{116}$$

with a computational effort of $\mathcal{O}(LS^3)$. Hence again the latter technique is suitable for small S, the former method becomes more and more advantageous if S increases, being clearly superior for $S = N$, but the turning point is higher then in the case of the coefficients themselves. It is found to be roughly $S \approx 100$ for $L = 12$.

If the components of B are determined from $\frac{\partial Q}{\partial B_{ij}} = 0$ their derivatives are not required (cf. Eq. (93)).

References

[1] L. Sirovich, Chaotic dynamics of coherent structures, Physica D 37 (1989) 126–145.
[2] L. Sirovich, Turbulence and the dynamics of coherent structures, Parts I–III, Q. Appl. Math. XLV (1987) 561.
[3] L. Sirovich, B.W. Knight and J.D. Rodriguez, Optimal low-dimensional dynamical approximations, Q. Appl. Math. XLVIII (1990) 535.
[4] J.D. Rodriguez and L. Sirovich, Low-dimensional dynamics for the complex Ginzburg–Landau equation, Physica D 43 (1990) 77–86.
[5] N. Aubry, P. Holmes, J.L. Lumley and E. Stone, The dynamics of coherent structures in the wall region of a turbulent boundary layer, J. Fluid Mech. 192 (1988) 115–175.
[6] F.M. Selten, Toward an optimal description of atmospheric flow, J. Atmos. Sci. 50 (1993) 861–877.
[7] F.M. Selten, An efficient description of the dynamics of barotropic flow, J. Atmos. Sci. 52 (1995) 915–936.
[8] M. Kirby, Minimal dynamical systems from PDEs using Sobolev eigenfunctions, Physica D 57 (1992) 466–475.
[9] C. Uhl, R. Friedrich and H. Haken, Reconstruction of spatio-temporal signals of complex systems, Z. Phys. B 92 (1993) 211–219.
[10] C. Uhl, R. Friedrich and H. Haken, Analysis of spatio-temporal signals of complex systems, Phys. Rev. E, in press.
[11] R. Friedrich and C. Uhl, Spatio-temporal Analysis of Human Electroencephalograms: Petit-Mal Epilepsy, to be published.
[12] V.K. Jirsa, R. Friedrich and H. Haken, Reconstruction of the spatio-temporal dynamics of a human magnetoencephalogram, to be published.
[13] U. Achatz, G. Schmitz and K.-M. Greisiger, Principal interaction patterns in baroclinic wave life cycles, J. Atmos. Sci., in press.
[14] K. Hasselmann, PIPs and POPs: the reduction of complex dynamical systems using principal interaction and oscillation patterns, J. Geophys. Res. 93 (1988) 11015–11021.
[15] H. von Storch, G. Bürger, R. Schnur and J.-S. von Storch, Principal oscillation patterns: a review, J. Climate 8 (1995) 377–400.
[16] J. Pedlosky, Geophysical Fluid Dynamics, 2nd. Ed. (Springer, New York, 1987) 710 pp.
[17] M. Ghil and S. Childress, Topics in Geophysical Fluid Dynamics: Atmospheric Dynamics, Dynamo Theory, and Climate Dynamics (Springer, New York, 1987) 485 pp.
[18] J.R. Holton, An Introduction to Dynamic Meteorology, 3rd Ed. (Academic Press, 1992) 511 pp.
[19] S.A. Orszag, Transform method for calculation of vector-coupled sums: Application to the spectral form of the vorticity equation, J. Atmos. Sci. 27 (1970) 890–895.
[20] B. Machenhauer, Spectral methods, Proc. Numerical Methods in Atmospheric Models, Shinfield Park, Reading, UK, ECMWF (1991) 3–85.
[21] I. Shimada and T. Nagashima, A Numerical Approach to Ergodic Problem of Dissipative Dynamical Systems, Prog. Theor. Phys. 61 (1979) 1605.
[22] R.W. Preisendorfer, Principal component analysis in meteorology and oceanography (Elsevier, Amsterdam, 1988) 401 pp.
[23] G.R. North, T.L. Bell, R.F. Cahalan and F.J. Moeng, Sampling errors in the estimation of empirical orthogonal functions, Mon. Wea. Rev. 110 (1982) 699–706.
[24] A.K. Louis, Inverse und schlecht gestellte Probleme (Teubner, Stuttgart, 1989) [in German].
[25] A. Tarantola, Inverse Problem Theory (Elsevier, 1987) 613 pp.
[26] L.M. Delves and J.L. Mohamed, Computational Methods for Integral Equations (Cambridge Univ. Press, 1985).
[27] P.E. Gill, W. Murray and M.H. Wright, Practical Optimization (Academic Press, London and New York, 1981) 401 pp.
[28] I.M. Navon and D.M. Legler, Conjugate-gradient methods for large-scale minimization in meteorology, Mon. Wea. Rev. 115 (1987) 1479–1502.